University of Alberta

Development of a Novel Polyurethane Lined Composite Pipe

by

Kulvinder Juss 

A thesis submitted to the Faculty of Graduate Studies and Research
in partial fulfillment of the requirements for the degree of

Master of Science
in
Applied Mechanics

Department of Mechanical Engineering

Edmonton, Alberta
Fall 2008

Library and
Archives Canada

Published Heritage
Branch

395 Wellington Street
Ottawa ON K1A 0N4
Canada

Bibliothèque et
Archives Canada

Direction du
Patrimoine de l'édition

395, rue Wellington
Ottawa ON K1A 0N4
Canada

Your file Votre référence
ISBN: 978-0-494-47274-3
Our file Notre référence
ISBN: 978-0-494-47274-3

NOTICE:
The author has granted a non-exclusive license allowing Library and Archives Canada to reproduce, publish, archive, preserve, conserve, communicate to the public by telecommunication or on the Internet, loan, distribute and sell theses worldwide, for commercial or non-commercial purposes, in microform, paper, electronic and/or any other formats.

The author retains copyright ownership and moral rights in this thesis. Neither the thesis nor substantial extracts from it may be printed or otherwise reproduced without the author's permission.

AVIS:
L'auteur a accordé une licence non exclusive permettant à la Bibliothèque et Archives Canada de reproduire, publier, archiver, sauvegarder, conserver, transmettre au public par télécommunication ou par l'Internet, prêter, distribuer et vendre des thèses partout dans le monde, à des fins commerciales ou autres, sur support microforme, papier, électronique et/ou autres formats.

L'auteur conserve la propriété du droit d'auteur et des droits moraux qui protège cette thèse. Ni la thèse ni des extraits substantiels de celle-ci ne doivent être imprimés ou autrement reproduits sans son autorisation.

In compliance with the Canadian Privacy Act some supporting forms may have been removed from this thesis.

While these forms may be included in the document page count, their removal does not represent any loss of content from the thesis.

Conformément à la loi canadienne sur la protection de la vie privée, quelques formulaires secondaires ont été enlevés de cette thèse.

Bien que ces formulaires aient inclus dans la pagination, il n'y aura aucun contenu manquant.

Canada

Abstract

It has been observed that traditional metallic pipelines used for oil sands slurry transport have a limited lifespan of only six months in some cases. These pipes experience excessive internal abrasion from high velocity sand particles and are subjected to internal corrosion from chemical solvents in the aqueous and aerated slurry flow. The objective of the current research study was to establish preliminary experimental and analytical framework for the development of a polyurethane-lined fiber-reinforced composite tubular, which is free of liner collapse and resistant to abrasion/corrosion. This was accomplished through:

- Mechanical testing of the polyurethane liner;
- Establishing a fabrication procedure for the manufacturing of small-scale lined composite pipes;
- Performing preliminary experimental testing on the developed pipe specimens;
- Optimizing the pipe manufacturing process through an experimental fracture investigation;
- Development of a finite element analysis to model fracture initiation at the polyurethane-epoxy interface.

Acknowledgments

This work would not have been possible without the patience and support of my supervisor and colleague, Dr. Pierre Mertiny. I would also like to thank the following for financial, material and technical contributions: the Department of Mechanical Engineering, Syncrude Canada, Kemenny Vek, Normac Adhesives, and Mr. Bernie Faulkner. I am also grateful to my family, particularly Ms. Heather Lockie, for their constant encouragement throughout this endeavor.

Table of Contents

List of Tables

List of Figures

List of Nomenclature

Roman Symbols

A_o	Undeformed initial cross section of tensile test specimen
a	Debond radius
C_1	Mooney-Rivlin constant 1
C_2	Mooney-Rivlin constant 2
E	Young's modulus
F	Applied tensile force
F_A	Applied axial load
G	Shear modulus
G_{cn}	Cohesive separation energy or work of fracture
h	Thickness
H_c	Blister height at the critical pressure
ID	Internal pipe diameter
L	Instantaneous length of tensile test specimen
L_o	Initial length of tensile test specimen
P	Pressure
P_c	Critical pressure
P_c^*	Non-dimensional critical pressure
P_i	Internal pipe pressure
P_o	Atmospheric pressure
R	Pipe radius

t	Pipe wall thickness
u_c^n	Critical normal displacement at complete debonding

Greek Symbols

Δ	Debond displacement
ϵ	True strain
ϵ_e	Engineering strain
Γ	Fracture strength
λ	Extension ratio
ν	Poisson's ratio
σ	True stress
σ_{axial}	Axial stress
σ_e	Engineering stress
σ_{hoop}	Hoop stress
σ_{max}	Maximum cohesive tensile strength

Abbreviations

ASTM	American Society for Testing and Materials
CZM	Cohesive zone model
DIC	Digital image correlation
FMEA	Failure mode and effects analysis
FRPC	Fiber-reinforced polymeric composite
HDPE	High-density polyethylene
LVDT	Linear variable displacement transducer
PE	Polyethylene
PTFE	Poly(tetrafluoroethylene)
PU	Polyurethane
PVC	Polyvinyl chloride
TDI	Toluene diisocyanate

Chapter 1

Introduction

1.1 Background of the Current Study

According to the Alberta Department of Energy northern Alberta holds approximately 173.2 billion barrels of proven oil reserves, which is second only to Saudi Arabia [1]. However, unlike conventional hydrocarbon reserves found in the Middle East and elsewhere, the crude oil deposits in Alberta are trapped within sand and clay, and consequently must be separated out. The oil sands are mined and transported to processing plants where bitumen, a heavy and viscous form of crude oil, is extracted. The pipelines used to transport oil sands slurry, which consist of bitumen, sand, clay, water and various chemicals, to and from processing plants undergo severe erosion-corrosion as a result of the internal abrasion due to sand particles and chemical corrosion from additives such as sodium hydroxide. With increasing industry investment in oil sands development, bitumen production is expected to almost triple by the year 2016 [2]. Consequently, slurry transport pipelines face escalating mainte-

This chapter is an updated and revised version of that which appeared in the 2008 Canadian Society for Mechanical Engineering conference paper "Fabrication and Performance of a Novel Polyurethane-Lined Fiber-Reinforced Composite Pipe," by Kulvinder Juss and Pierre Mertiny.

nance and replacement costs. As such, there is a demand for piping structures that have superior abrasion and corrosion resistance properties, and ultimately a longer lifespan.

1.2 Review of Pipeline Technology

According to [5] these pipelines common to the industry have a lifespan of between six weeks and six months, depending on slurry flow properties and pipeline surface treatment. To reduce internal damage caused by the erosion-corrosion phenomenon, metallic pipelines are often internally clad through the process of thermal spraying. In thermal spraying, high temperature atomized particles of feedstock material are deposited onto the inside surface of the pipe as a means of altering the immediate substrate properties to obtain favorable abrasion and corrosion characteristics. The feedstock can be composed of wide ranging materials, including ceramics, but are typically metals such as zinc, aluminum and tungsten. As the high velocity feedstock particles impact the pipe substrate, they flatten out, cool, and eventually build up to form a protective coating [3]. The capability of the protective coating to shield the underlying piping is dependent on numerous variables such as the surface preparation, processing environment and feedstock composition [4]. Although thermal spraying increases the lifespan relative to untreated pipes, it has had limited success in drastically prolonging the usefulness of highly erosive-corrosive slurry transportation lines. Furthermore, the process of thermal spraying pipelines is particularly expensive in terms of: the cost for exotic feedstock material, surface preparation, and the energy input required to vaporize the feedstock.

In the United States, it has been estimated that metallic pipeline (gas, sewer, and water) related corrosion costs the economy upwards of 40 billion dollars annually [6]. Furthermore, in Alberta alone, 65% of all pipeline failures are caused by internal or

external corrosion [7]. Polymeric materials are considered to have better abrasion and corrosion resistance relative to metals and are thus becoming increasingly used within the pipeline industry. Internally coating metallic tubulars with a sacrificial polymeric liner is a cost-effective method of combining the strength characteristics of steel and the wear/corrosion properties of a polymer. In this process, which is similar to spin casting, the pipe is constantly rotated while a liquid polymer is centrifugally cast and cured onto the inside surface. A variant of this process involves inserting a pre-formed and fully cured polymeric liner into a metal pipe and adhesively bonding the entities. However, it has been found that these piping systems are prone to liner collapse when used in pressurized environments that contain hydrocarbons. Over time hydrocarbon volatiles can permeate through the polymer coating and collect at the metal-liner interface [8]. Although this is not problematic during normal operating conditions, it can be devastating under an irregular pipeline operation such as a sudden depressurization. Depressurization of the liner interior will create an imbalance in force relative to the pressurized fluid at the interface; this pressure difference may lead to catastrophic liner buckling or collapse. As re-pressurization of the pipe interior occurs and the polymeric liner expands, it becomes prone to ripping. This can allow corrosive and abrasive fluid into the annulus between the host pipe and the liner itself, and ultimately lead to the pipe's failure; moreover, it is difficult to predict when or where such a collapse will occur. Figure 1.1 illustrates the concept of liner collapse, where P, Δ, h, and R are the annular pressure, debond displacement, liner thickness and pipe radius, respectively.

Theoretical attempts to analyze liner collapse generally rely on the following equation, which is based upon two-dimensional plane strain formulation [8]:

$$P_c^* = \frac{P_c(1-\nu^2)}{E} = A\frac{h}{R}^n \tag{1.1}$$

This equation presents the critical pressure required for liner collapse, P_c, in the

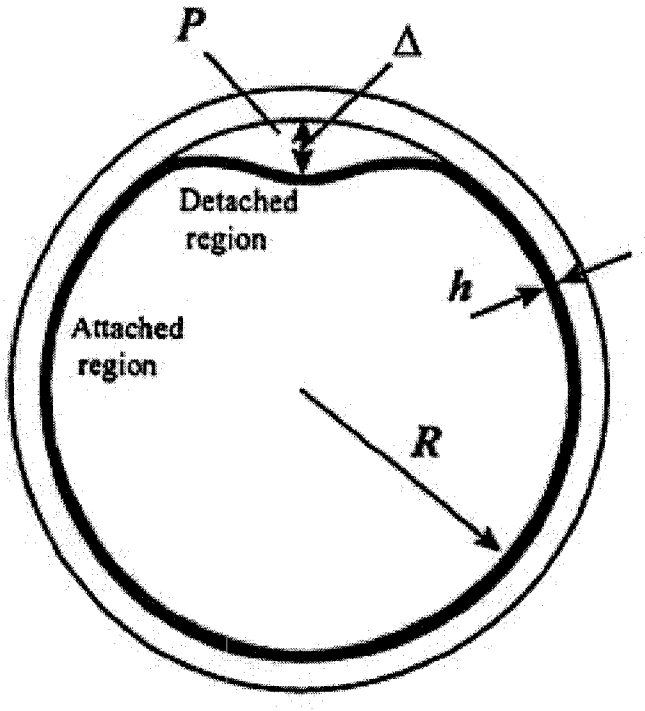

Figure 1.1: Collapse of a polymeric liner(adopted from [8])

non-dimensional form of P_c^* which relates to the liner's modulus of elasticity, E, and Poisson's ratio, ν. Furthermore, the parameters A and n are dependent on the boundary conditions between the liner and host pipe, and generally range between of 0.2-0.4 and 2-3, respectively; exact values for these constants can be found in [8]. Based upon the above equation, the critical pressure can be initially maximized by altering the pipe sizing and liner material properties and thickness, however, one must also account for progressive changes in the pipe during normal pipeline operations. These variables include reduction in liner thickness as material is lost to abrasion and a change in the elastomeric properties as the polymer swells and degrades due the presence of hydrocarbons and corrosive environment. Since the values of these parameters are generally unknown, it can be difficult to optimize the critical collapse pressure for real-life conditions.

An alternative method of reducing the likelihood of liner collapse can be achieved

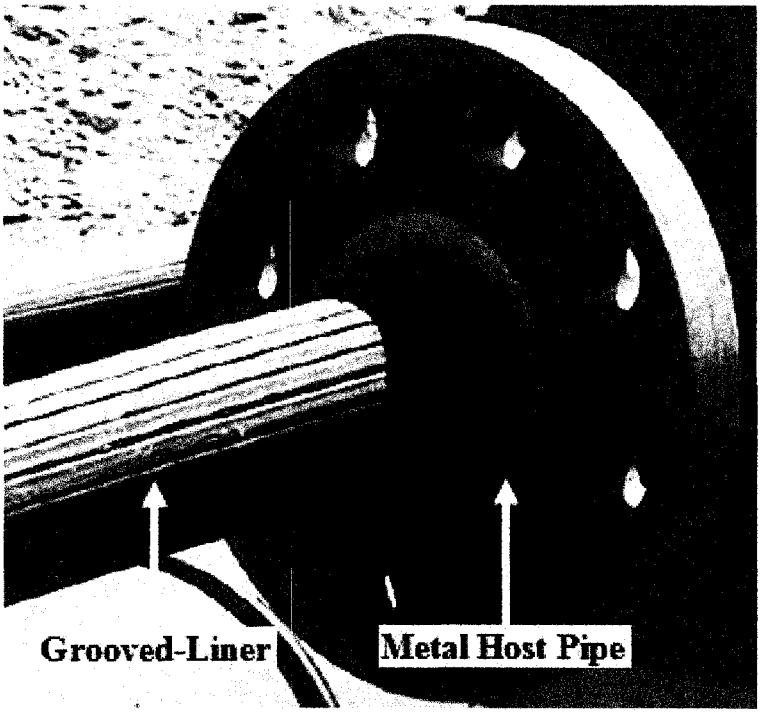

Figure 1.2: Insertion of a grooved liner into the host metallic pipe (adopted from [10])

by venting the trapped interfacial volatiles. Such a pipe was proposed in [9] and in this setup, a longitudinally grooved thermoplastic liner is inserted into a host metallic pipe, shown in Figure 1.2. The grooves along the polymeric liner channel any gases that have accumulated due to hydrocarbon permeation to a series of outlet valves located along the pipeline, thus eliminating the potential for collapse. However, such piping systems have questionable long-term functionality, restricted pipe length and may significantly increase the cost of manufacturing and field installation.

Although internal polymeric liners reduce internal abrasion and corrosion, external corrosion of pipelines is still a significant issue as more than 10% of metal pipes fail in this way in the province of Alberta [7]. One option to overcome this concern is the implementation of fully polymeric pipelines. There are commercial products available (e.g. Flexpipe by Flexpipe Systems Inc.) which combine the corrosion resistance of HDPE and the strength of fiber-reinforcements, however, due to their spoolable nature

these systems can only be produced for use in small diameter applications, usually in the 5 to 13 centimeter (2 to 4 inch) region. Unfortunately, the pipelines used for slurry transport typically have diameters between 61 to 91 centimeters (24 to 36 inches). Furthermore, since the fiber-reinforcements utilized within this piping system are not bound within a thermoplastic or thermoset matrix their load carrying capability is reduced. Although fibers are the main load bearing component in a fiber-reinforced polymeric composite (FRPC), the matrix acts to (a) distribute stresses to the fibers and, (b) shield the fiber from environmental degradation. As such, pipelines which include dry fibers have a decreased pressure retaining capability and may be at an increased risk of failure relative to a comparable matrix impregnated FRPC pipe.

1.3 Overview of the Present Research

The objective of the current research study is to establish preliminary experimental and analytical framework for the development of a polyurethane-lined fiber-reinforced composite tubular, which is: (a) free from liner collapse, and (b) resistant to abrasion and corrosion. To accomplish this objective, this report has been sectioned into a four part paper series that will address:

1. Mechanical testing of the polyurethane material system;
2. Fabrication methodology and preliminary experimental testing of the developed lined composite pipes;
3. Optimization of the pipe manufacturing process through an experimental fracture investigation;
4. Development of a finite element analysis to model the fracture initiation of a PU-epoxy interface.

Bibliography

[1] Alberta Department of Energy, "Alberta's oil sands 2006," http://www.energy.gov.ab.ca/OilSands/pdfs/osgenbrf.pdf, updated Dec. 2007.

[2] Alberta Department of Energy, "Talk about oil sands," http://www.energy.gov.ab.ca/OilSands/pdfs/FS_OilSands.pdf, Jan. 2008.

[3] Westergaurd, R., Erickson, L.C., Axe, N., Hawthorne, H.M., Hogmark, S., "The erosion and abrasion characteristics of alumina coatings plasma sprayed under different spraying conditions," Tribology Internationa, vol. 31, no. 5, pp. 271-279, 1998.

[4] Hawthorne, H.M., Arsenault, B., Immarigeon, J.P., Legoux, J.G., Parameswaran, V.R., "Comparison of slurry and dry erosion behaviour of some HVOF thermal sprayed coatings," Wear, 225-229, pp. 825-834, 1999.

[5] Research group meeting with Syncrude Canada: May 16, 2008.

[6] Lees, J.M., "Behaviour of GFRP adhesive pipe joints subjected to pressure and axial loadings," Composites: Part A, vol. 37, pp. 1171-1179, 2006.

[7] Grzyb, D., "Spoolable composite pipeline usage in Alberta," http://igs.nigc.ir/igs/standard/ARTIC/PL-08.pdf, CGA Conference Presentation, 2006.

[8] Frost, S.R., Korsunsky, A.M., Wu, Y., Gibson, A.G., "Collapse of polymer and composite liners constrained within tubular conduits," Plastics, Rubbers and Composites, vol. 29, no. 10, pp. 568-572, 2000.

[9] Taylor, J., Groves, S., Melve, B., Frost. S.R., "Effective annular venting of thermoplastic liners for added value and benefit," 2000 NACE Corrosion Conference, Paper 00784.

[10] SafetyLiner Systems Canada Limited, Pipeline Integrity Management, `http://www.safetyliner.com/SafetylinerPipeIntegrityMgtS.pdf`. Retrieved on August 12, 2008.

Chapter 2

Material Characterization: Polyurethane Elastomer Tensile Testing

2.1 Introduction to Polymers

Polymers are a broad category of materials ranging from naturally occurring forms such as rubber and DNA, to synthetically manufactured polyester. According to [1], "a polymer is a substance composed of molecules which have long sequences of one or more species of atoms or groups of atoms linked to each other by covalent bonds," these molecules are often referred to as macromolecules. Macromolecules are created through chemical reactions or polymerization of monomers, which are small molecular chains. In general, however, polymers can be separated into three groups, namely thermoplastic, thermosetting and elastomeric; the underlying molecular structure of the solid polymer is the main distinguishing feature between the categories of polymers. Figure 2.1 illustrates the three types of skeletal structures that a polymer may have, namely linear, branched, and network.

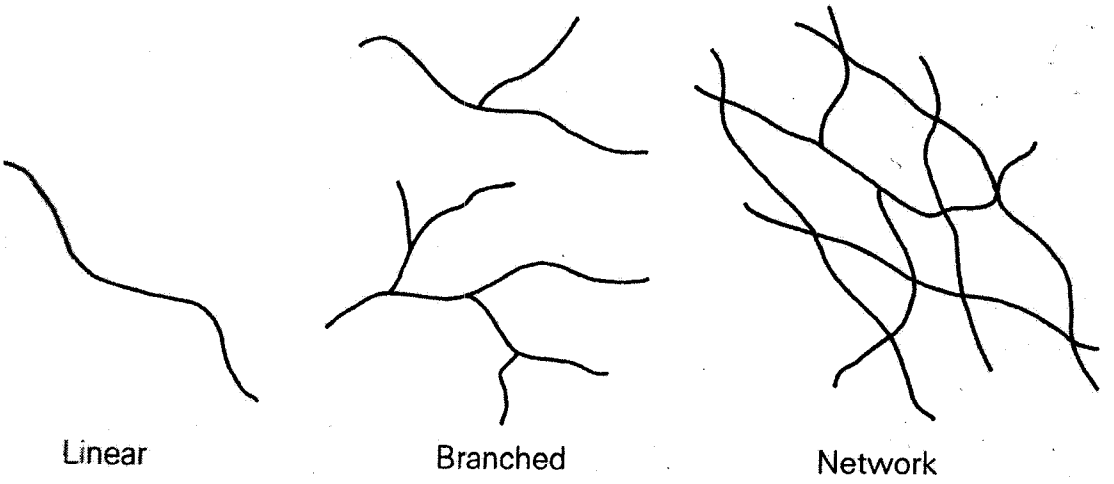

Figure 2.1: Polymer skeletal structures (adopted from [1])

Thermoplastics, which are either a linear or branched skeletal structure, can be indefinitely reshaped through melting and solidification. Thermoplastics can be further divided into amorphous and semi-crystalline polymers, with the main difference between the two being on the order of their molecular structure upon hardening. As an amorphous polymer solidifies it does not form an ordered molecular structure, which can be likened to a bowl of spaghetti [2]. Conversely, a semi-crystalline thermoplastic will form an ordered long-range molecular configuration as it is cooled below its melting temperature. Typical examples of an amorphous and a semi-crystalline thermoplastic polymers are polyvinyl chloride (PVC) and polyethylene (PE), respectively.

Unlike thermoplastics, thermosetting polymers and elastomers have the ability to chemically crosslink during the curing process. These crosslinks are formed between molecular chains and endow the polymer with the ability to resist melting upon heating. Thermosets form high-density crosslinked networks that do not allow the polymer molecules to move, consequently, they generally exhibit high stiffness and brittleness [3]. On the other hand, elastomers are only lightly crosslinked and allow for large and reversible deformation [3]. The properties of a polymer are not governed solely

by the underlying molecular skeletal structure. The molecular weight, confirmation, conformation and degree of polymerization all play an important role in defining the mechanical, optical, thermal and electrical characteristics of a polymer. A theoretical understanding of these basic tenets can be found in any introduction to polymers textbook, thus, they will not be discussed here.

The objective of this chapter is to experimentally evaluate the stress-strain behaviour of a polyurethane elastomer and compare the results to theoretical models. It is anticipated that the theoretical model which best fits the experimental data can ultimately be implemented into future finite element analysis which requires the modelling the behaviour of the polyurethane. As such, this section will: (a) provide an overview of polymer testing and relevant theoretical models, (b) describe the polyurethane material system, sample fabrication, experimental setup and testing procedures, and (c) present results of the experimental investigation and theoretical predictions.

2.2 Theory

Unlike traditional metallic materials which are generally considered to obey Hooke's law at low strains, polymers exhibit viscoelastic behaviour. Simply put, during deformation, viscoelastic materials display elements of both viscosity and elasticity. According to [4], the mechanical behaviour of a polymer can be described as being a hybrid of an elastic solid and a rate dependent liquid. At high strain rates and low temperatures, polymers will behave as an elastic solid; conversely, at low strain rates and high temperatures, polymers will flow like a liquid, thus exhibiting viscous characteristics. This suggests that the stress and strain seen by a polymer are a function of time and temperature. There are a number of experimental methods available to determine the mechanical characteristics of a given polymer, and can

generally be categorized into (a) long term tests or, (b) short term tests. The aim of long term tests, such as creep testing, stress relaxation testing and fatigue testing, is to interpret the underlying viscoelastic behaviour of the polymer. In contrast, short term tests are concerned with determining stress-strain behaviour and fundamental material properties such as rigidity and Poisson's ratio. As these are the quantities sought in this investigation, only short term testing will be discussed in this paper.

Tensile, compression and shear tests are typical short term test methods used to determine material properties. These methods can be further categorized into fundamental, component and hybrid tests [5]. The experimental data gathered from fundamental tests are independent of the specimen geometry and experimental testing equipment. Conversely, component testing is used to determine the specimen behaviour while undergoing real world conditions. Lastly, hybrid tests are a combination of fundamental and component testing. Fundamental uniaxial tensile testing will be performed on the polyurethane elastomer to determine its stress-strain behaviour, Young's modulus and Poisson's ratio.

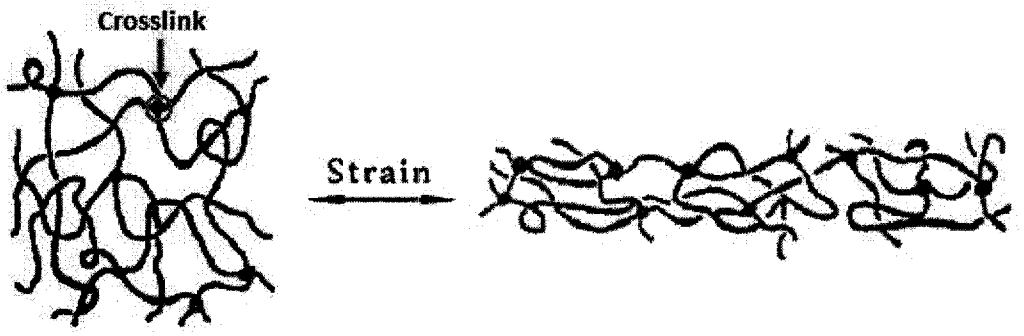

Figure 2.2: Elastomer under uniaxial stress (adopted from [6])

The uniaxial tensile testing is the most utilized mechanical testing method. In this test, the specimen is loaded either through applying a constant rate of deformation or through a constant increase in load; however, in terms of practicality the first option is usually selected. One of the major advantages of elastomers is their incredible ability

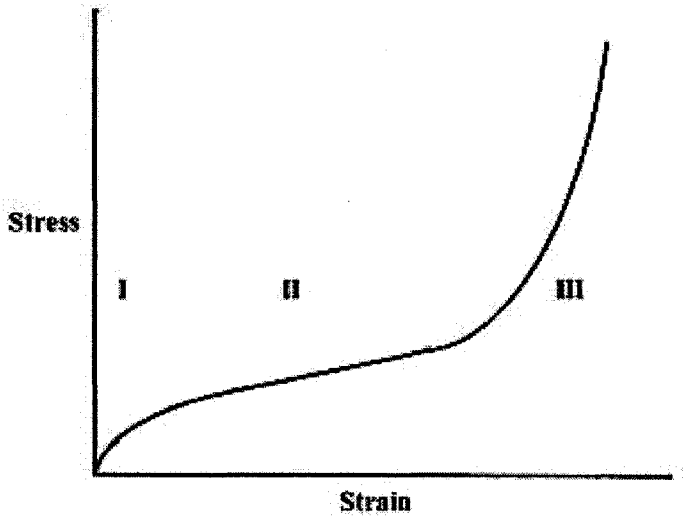

Figure 2.3: Typical true-stress-strain curve for an elastomer

to stretch without incurring permanent deformation. During uniaxial deformation, the molecular chains uncurl and extend; however, the lightly crosslinked network, which is present in elastomers, inhibits the macromolecules from permanently sliding past each other [7]. Once the loading has been removed the majority of polymer chains return to their original unperturbed positions, Figure 2.2 illustrates this concept.

Figure 2.3 displays a typical stress-strain curve for an elastomeric material. There are three distinct regions visible in this graph. Initially there is an elastic region, which is typical of most stress-strain curves, here Hooke's law is obeyed, and the deformation is completely reversible. This region then transitions into a quasi-plateau, where there is a large increase in strain, but a minimal increase in stress. During this phase, the polymer chains uncurl and align themselves in the direction of deformation. Strain hardening occurs in region III as a result of the macromolecules all being aligned in the same direction, which provides considerable strength in the direction of elongation.

There are many theories which have been developed to predict the stress-strain behaviour of elastomeric or rubbery materials. The basis for these theories can range from thermodynamics and statistical mechanics to chemical structure and continuum

mechanics. However, theories based on statistical mechanics and continuum mechanics are the most popular, and as such they will be briefly outlined and utilized to model the polyurethane's experimentally determined stress-strain behaviour. Statistical mechanics directly analyzes changes in the molecular structure during loading [8]. For an elastomer undergoing uniaxial tension (or compression), this theory predicts that the engineering stress, σ_e, can be computed as a function of the extension ratio, λ [9, 10]. This prediction is given by:

$$\sigma_e = G(\lambda - \frac{1}{\lambda^2}) \tag{2.1}$$

The extension ratio is defined as the ratio of instantaneous length, L, to the initial length of the specimen, L_o, or $\lambda = \frac{L}{L_o}$; the extension ratio also relates the true stress, σ, to the engineering stress through: $\sigma_e = \frac{\sigma}{\lambda}$. Furthermore, by selecting an appropriate value for the modulus, G, the equation can be fit to experimental data.

The second class of theories, which is centered on a continuum mechanics approach, does not consider the molecular structure of the polymer. Instead, equations with a varying number of parameters are fit to a given stress-strain data set [11]. Such models are referred to as phenomenological theories, and are often popular with engineers and researchers who are not familiar with the theoretical polymer physics used in the derivation of statistical mechanics. The following two-parameter Mooney-Rivlin equation is a typical phenomenological model:

$$\sigma_e = 2(C_1 + \frac{C_2}{\lambda})(\lambda - \frac{1}{\lambda^2}) \tag{2.2}$$

This model is only valid for uniaxial loading, and assumes that the material is isotropic and incompressible [12]. The constants C_1, and C_2 are selected to best fit experimental data, furthermore, it should be noted that these coefficients are different for each material.

2.3 Experimental

2.3.1 Material System

The polymer under consideration is a castable polyurethane elastomer (NR-606M, Normac Adhesive Products) centered on a toluene diisocyanate (TDI) prepolymer, which is a 80:20 isomer blend of 2,4-TDI and 2,6-TDI, respectively. Figure 2.4a illustrates a 2,4-TDI monomer, while Figure 2.4b describes a reaction between diisocyanate with a polyol monomer containing functional hydroxyl (-OH) end groups which creates a generalized polyurethane molecule.

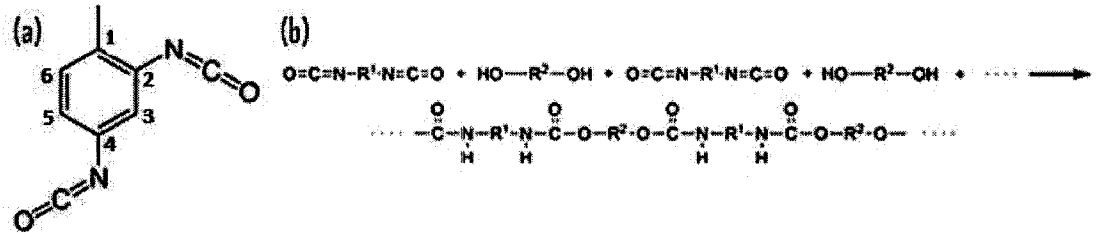

Figure 2.4: a) 2-4 TDI molecule b) Generalized polyurethane reaction (Public Domain Usage)

2.3.2 Sample Fabrication

The liquid PU was pneumatically injected into an aluminum mould to form specimens with dimensions shown in Figure 2.5, these dimensions are in accordance with ASTM D638-03 standard test method for determining the tensile properties of plastics [13]. The mould was then placed into an oven preheated to 82.2°C and fully cured for 5 hours. Following curing, the specimens were removed from the oven and allowed to return to room temperature.

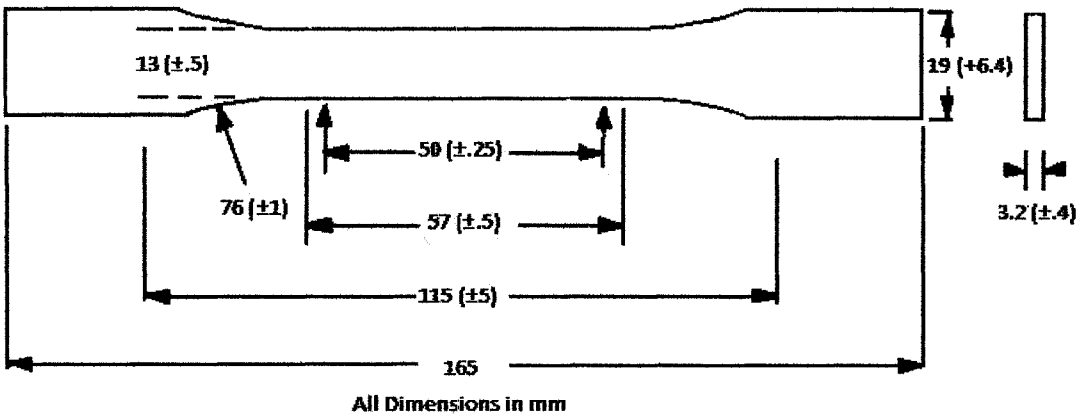

Figure 2.5: Dimensions of tensile test specimens (adopted from [13])

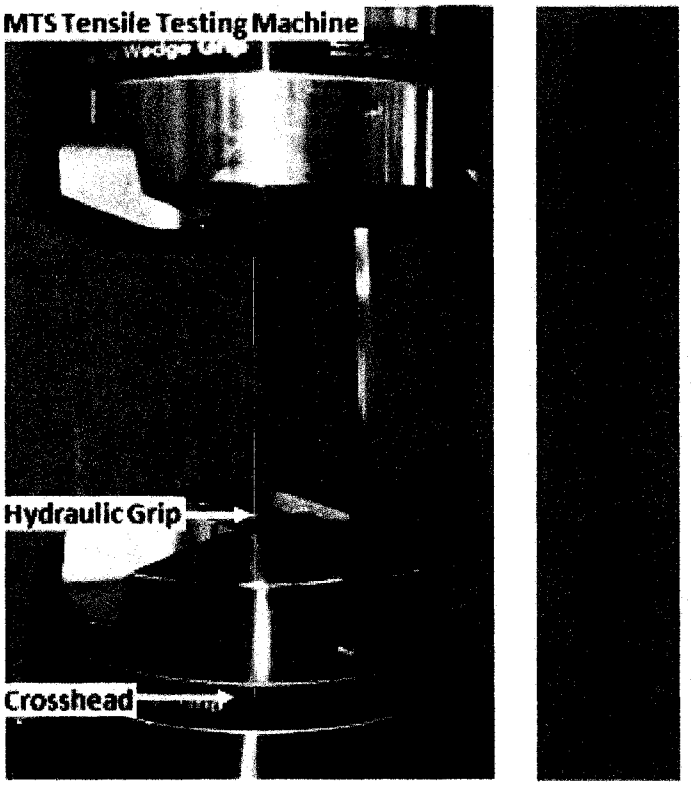

Figure 2.6: left) MTS testing machine, right) PU tensile test specimen

2.3.3 Experimental Setup and Testing Procedure

Specimens were placed into the MTS tensile testing, and secured in the top and bottom crossheads using a set of hydraulic grips shown in Figure 2.6. During testing, the top crosshead remained stationary while the bottom crosshead extended vertically downward at the ASTM D638-03 suggested rate of 50 mm/minute. A total of ten specimens were tested; five to determine the modulus of elasticity and five to determine Poisson's ratio. As high extension strain gauges and extensometer are currently not available, the axial strain behaviour was obtained by using stroke data recorded during the experiment. This technique has also been used within literature and was found to only slightly underestimate the stiffness of the material compared to results obtained through use of a laser extensometer [14]. Similarly, to determine the Poisson's ratio, a digital vernier caliper was utilized to periodically measure the change in the specimen's width.

2.4 Results

Figure 2.7 illustrates typical true stress-strain and engineering stress-strain curves for the polyurethane. The engineering stress was computed simply by dividing the digitally recorded applied force, F, by the undeformed initial cross section, A_o. To determine the true stress, σ, which accounts for changes in the specimen's cross-section, Equation 2.3 was used [14].

$$\sigma = \sigma_e(1 + \epsilon_e) \tag{2.3}$$

The true strain (also called the Hencky strain), ϵ, was computed through the following equation [14]:

$$\epsilon = ln(1 + \epsilon_e) \tag{2.4}$$

The modulus of elasticity was established based on the initial linear-elastic slope of the stress-strain curve as displayed in Figure 2.7. The average Young's modulus over five experiments was determined to be 21.5±2.4 MPa. The engineering strain, ϵ_e, was obtained by dividing the stroke by the initial gauge length of the specimen, which is the unstretched distance between the upper and lower hydraulic grips. The mean Poisson's ratio was determined to be 0.44±0.01, and was calculated by dividing the transverse strain obtained from the change in the specimen's width by the corresponding engineering axial strain.

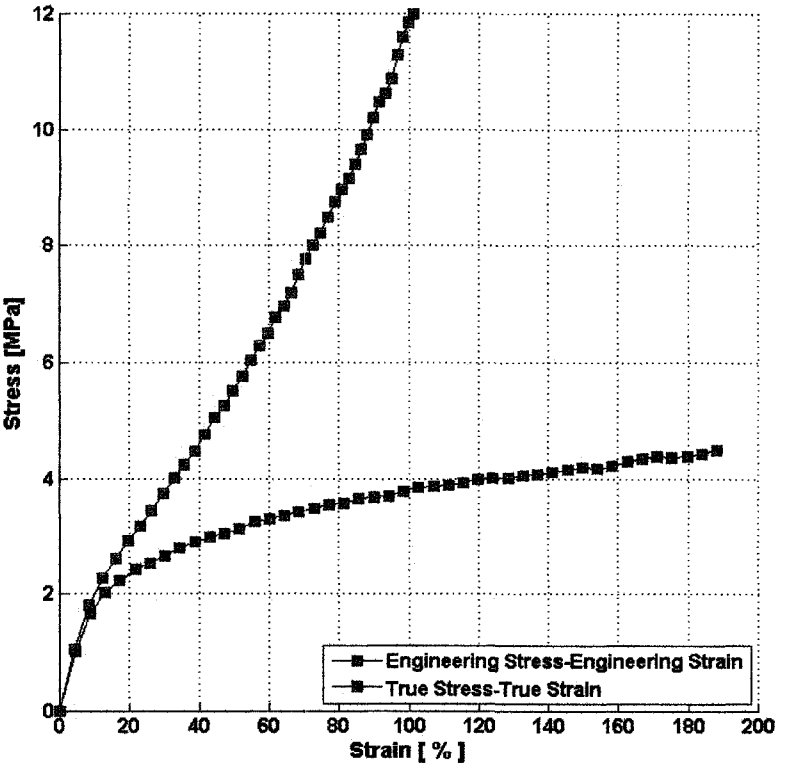

Figure 2.7: Comparison between engineering stress-strain and true stress-strain

The following figure illustrates the comparison between the theoretical models presented earlier and experimental data. The two-parameter Mooney-Rivlin model implements coefficients of C_1=-0.21 MPa and C_2=2.7 MPa, while the statistical me-

chanics based model employs a modulus of G=7.167 MPa.

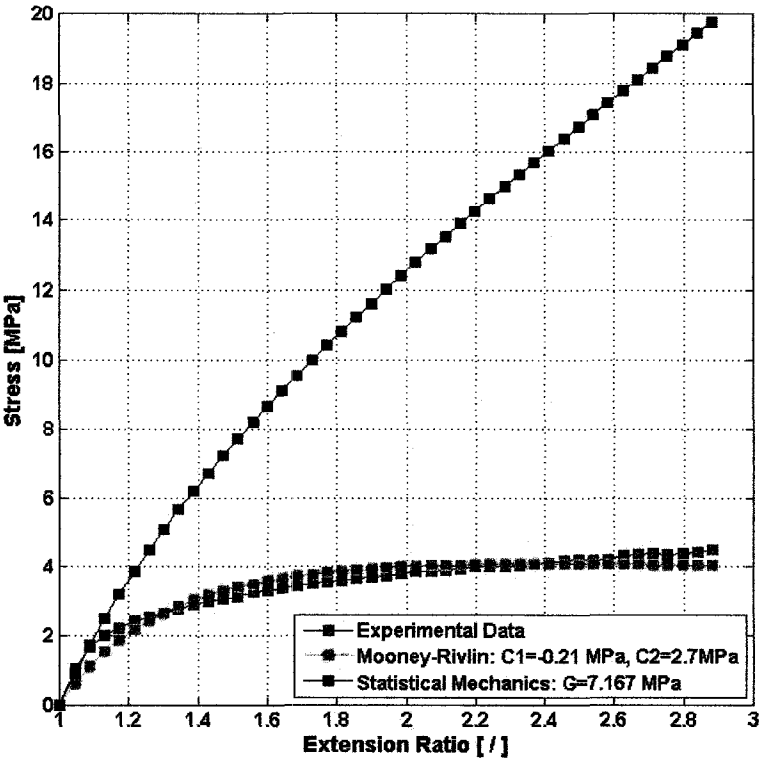

Figure 2.8: Comparison between experimental engineering stress-strain data, statistical mechanics prediction and two parameter Mooney-Rivlin equation

2.5 Discussion

The average Young's modulus was determined to be 21.5±2.4 MPa; this value is on par with typical elastomer elastic moduli [9]. As expected the true stress-strain and the engineering stress-strain curves are essentially equivalent to roughly 15% strain, however, after this point, they become increasingly divergent. The main cause for this is that the true stress-strain curve accounts for the change in the polyurethane's cross-section as the sample is uniaxially stretched. It is also interesting to observe the difference between the true stress-strain curve in Figure 2.3 and Figure 2.7, namely

that there is no visible plateau in the experimental data; instead the sample transitions completely from linearly elastic to fully strain hardened. This may be a consequence of utilizing a relatively fast rate of deformation. It should also be noted that none of the specimens fractured or failed during testing; the tests were terminated because the MTS testing machine reached its stroke limit.

To determine the Poisson's ratio the testing machine was paused roughly after the specimen increased in length by 10mm which corresponds to approximately 10% axial strain and is within the polyurethane's elastic region. The main disadvantage of determining the Poisson's ratio in this fashion is that the testing must be suspended to allow for measuring the change in cross-sectional width, although these stoppages typically lasted less than 10 seconds, the molecular chains could potentially undergo relaxation during this period, thus introducing time dependency into the result. Polyurethane materials are considered to be nearly incompressible, meaning they have a Poisson's ratio of close to 0.5 [15]. However, the results of the current experimental investigation estimate the Poisson's ratio to be approximately 0.44 ± 0.01. It is suspected that this descrepancy is caused by compliance in the axial stroke data obtained from the testing machine. To overcome these difficulties, future analysis should be conducted with a non-contacting digital imaging measurement system, however, for the present engineering analysis this value is sufficient.

The statistical mechanical model predicts the initial slope very well, but completely fails after an extension ratio of 1.2. Conversely, the continuum based Mooney-Rivlin model is significantly better at modeling the overall shape of the curve. It is anticipated that the Mooney-Rivlin parameters can be implemented into future finite element analysis to model the non-linear behaviour of the polyurethane.

2.6 Conclusion

This chapter outlined the basic theory of uniaxial tensile testing of elastomeric materials. Tensile testing was performed on a polyurethane elastomer; samples were shaped according to the ASTM D638-03 standard. Based the experimental results, the modulus of elasticity and Poisson's ratio were determined to be 21.5 MPa and 0.44, respectively. Furthermore, two theoretical models were presented and compared to experimental stress-strain data. Of the two models presented, it was found that the two-constant Mooney-Rivlin continuum model was better at describing the stress-strain behaviour of the polyurethane; it is anticipated that these parameters can be implemented into future finite element analysis.

Bibliography

[1] Young, R.J., Lovell, P.A., "Introduction to polymers, 2nd edition," UK: Chapman and Hall, pp. 3, 1991.

[2] Osswald, T.A., Menges, G., "Materials science of polymers for engineers," Canada: Hanser Publications Inc., pp. 32, 1995.

[3] Osswald, T.A., Menges, G., "Materials Science of polymers for engineers," Canada: Hanser Publications Inc., pp. 11, 1995.

[4] Young, R.J., Lovell, P.A., "Introduction to polymers, 2nd edition," UK: Chapman and Hall, pp. 322, 1991.

[5] Brostow, W., "Performance of plastics," Canada: Hanser Publications Inc., pp. 104, 2000.

[6] Gerard, J.F., Meisel, I., Kniep, C. S., "Fillers and filled polymers: presentations at the conference Eurofillers '99," France: Wiley-VCH, pp. 248, 2001.

[7] Osswald, T.A., Menges, G., "Materials science of polymers for engineers," Canada: Hanser Publications Inc., pp. 255, 1995.

[8] Young, R.J., Lovell, P.A., "Introduction to polymers, 2nd edition," UK: Chapman and Hall, pp. 350, 1991.

[9] Young, R.J., Lovell, P.A., "Introduction to polymers, 2nd edition," UK: Chapman

and Hall, pp. 355, 1991.

[10] Osswald, T.A., Menges, G., "Materials science of polymers for engineers," Canada: Hanser Publications Inc., pp. 257, 1995.

[11] Brostow, W., "Performance of plastics," Canada: Hanser Publications Inc., pp. 413, 2000.

[12] Gedde, U.W., "Polymer physics," Canada: Springer, pp. 51, 2001.

[13] American Society for Testing and Materials, "Standard test method for tensile properties of plastics," ASTM D638, 2003.

[14] Arriagaa, A., Lazkanoa, J.M., Pagaldaia, R., Zalduaa, A.M., Hernandeza, R., Atxurraa, R., Chrysostomoub, A., "Finite-element analysis of quasi-static characterisation tests in thermoplastic materials: experimental and numerical analysis results correlation with ANSYS," Polymer Testing, vol. 26, pp. 284305, 2007.

[15] Vossoughi, J., "Determination of the Mooney material constants for highly nonlinear isotropic incompressible materials under large elastic deformations," Experimental Techniques, vol. 19, pp. 24-27, 1995.

Chapter 3

Fabrication and Performance of a Polyurethane Lined Composite Pipe

3.1 Introduction

This chapter is part of a larger research project on the development of a continuous and cost-effective fiber-reinforced polymeric composite pipe system suitable for slurry transport applications, and which is abrasion/corrosion resistant and free of liner collapse. Fabrication of this small-scale pipe involves filament-winding epoxy coated basalt fibers onto either: (1) a fully cured polyurethane liner, or (2) a partially cured polyurethane liner. The main difference between the two options is the type of interfacial bond; the former creates a mechanical bond, while the latter forms a chemical bond. Mechanical interlocking occurs when the substrate has a porous surface which

This chapter is a revised and updated version of that which appeared in the 2008 Canadian Society for Mechanical Engineering conference paper "Fabrication and Performance of a Novel Polyurethane-Lined Fiber-Reinforced Composite Pipe," by Kulvinder Juss and Pierre Mertiny.

allows uncured adhesive to penetrate before hardening. Chemical adhesion is centered on the formation of ionic bonds, hydrogen bonds or covalent bonds across the bond line. The proposed design can potentially overcome venting difficulties seen in lined steel pipes by utilizing networks of micro matrix cracks in the composite structure as a conduit to expel trapped interfacial volatiles into the atmosphere.

The objective of this section is to: (a) develop manufacturing procedures under laboratory conditions and, (b) provide preliminary experimental results comparing the failure behaviour of unlined to lined basalt-reinforced composite tubulars subjected to biaxial loading. Furthermore, this study also aims to elucidate if the type of interfacial bonding (mechanical vs. chemical) between the polyurethane liner and composite pipe has an influence on the results.

3.2 Pipe Structure and Theory

The prototype pipe consists of two main components: (a) the FRPC pipe, and (b) the polymer liner. The fiber-reinforced polymeric composite is the structural support of the piping system, as such; it is expected to support all loading during operation. Significant work on the failure behaviour of filament-wound composite tubulars has been conducted by scientists at the author's research group. It was observed that under biaxial loading conditions caused by axial tractions and internal pressurization, FRPC tubes usually fail in two defined modes, namely, fiber-fracture, and weepage. Fiber-fracture, which is the more severe of the two failures, causes highly pressurized composite pipes to burst. Weepage failure generally occurs at lower pressures and is initiated by the formation of networks of micro matrix cracks; these networks serve as passageways to allow interior pressurized fluids to escape. However, unlike fiber-fracture which induces complete structural failure, pipes undergoing weepage still maintain significant strength, but are simply unable to contain fluid [1]. In the

proposed pipe, leakage of internal fluids is overcome by introducing an internal polymeric liner, which also serves to shield the FRP structural component from damage caused by the abrasive and corrosive liquid slurry flow.

As mentioned previously, during normal pipeline operation hydrocarbon volatiles will eventually permeate through the polymer liner, and require venting to avoid liner collapse. It is proposed that venting be accomplished through an initial pipe commissioning process; during this procedure, the pipe would be conditioned through controlled internal pressurization to produce a uniform network of micro-matrix cracks in the composite structure. These pathways would allow diffusive volatiles to escape into the surroundings while the polymeric liner would prevent fluid leakage.

Since it is conceivable that the micro-matrix cracks used for venting volatiles may also allow external fluids into the pipe, it is important that external pressures do not exceed those found within the interior of the pipe. Generally, slurry transport pipes operate with internal pressures in the range of 2.4 MPa (350 psi) which is significantly greater than the atmospheric pressures experienced by aboveground. However, in case of irregular operation where external pressures do in fact surpass internal pressures, it is imperative that a strong adhesive bond between the composite pipe and the polymer liner exists.

NR-606M castable polyurethane from Normac Adhesive Products is used as the polymeric lining material for its superior abrasion and corrosion resistance characteristics. It is based on a two-constituent diisocyanate-ether formulation and cures to a Shore A hardness of 80±5. The two-component thermoset epoxy resin is centered on a bisphenol A formulation with an amine curing agent (EPON826 and EPICURE9551 from Hexion Specialty Chemicals). As mentioned previously, this study will examine tubulars that have liners which are either: a) mechanically bonded, or b) chemically bonded to the composite structure. To achieve a mechanical bond between the liner and the composite structure, the polyurethane elastomer is fully cured prior to

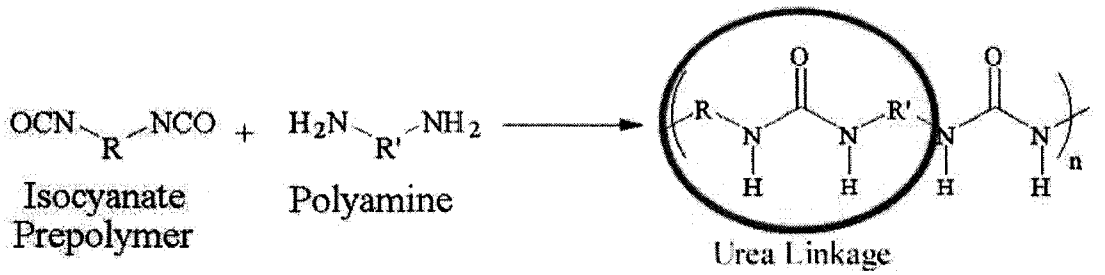

Figure 3.1: Generalized polyurea reaction (Public Domain Usage)

filament winding epoxy-impregnated basalt. Thus, all functional isocyanate groups within the polyurethane would be consumed, and consequently, unable to chemically react with the amine within the epoxy resin. In order to achieve a chemical bond between the liner and the composite pipe, the filament winding process is undertaken when the polyurethane is in a semi-cured state. This technique forms covalent interfacial chemical bonds by allowing amine groups in the epoxy resin to react with isocyanate groups in the uncured urethane, thus forming a polyurea compound at the interface. Figure 3.1 illustrates this generalized reaction.

Chemical bonding has been shown to improve adhesive bond strength by: (a) inhibiting molecular slippage during interfacial fracture, and (b) enhancing interfacial attraction, which in turn increases fracture energy [2]. Although interfacial chemical bonds have greater toughness compared to mechanically bonded joints, the manufacturing of such a chemical bond adds significant complexity to the overall fabrication process. The main difficulty is in determining the optimal cure time, which is a trade off between urethane firmness in the semi-cured state and chemical reactivity with the epoxy. The rigidity of the semi-cured polyurethane liner must be sufficient such that tears and cleavages are avoided during handling and filament winding, but there must also be adequate amounts of isocyanate present to react with functional amine groups.

In order to determine the optimal cure time, a cure rate analysis was completed. Measuring rate of cure is categorized into two methods: (a) direct, and (b) indirect

[3]. Direct methods include spectroscopy, thermal and acoustical analysis; these techniques are often expensive, complicated and require highly specialized equipment. Indirect methods are usually quick and simple to perform, and generally focus on measuring physical characteristics of the material. This study has adopted the indirect technique of hardness testing, which measures the polyurethane's resistance to indentation using a Shore A hardness durometer.

Ten samples of polyurethane were cured at 82.2°C (180°F). The hardness was measured every 30 minutes until no discernible change relative to the previous measurement was detected. Average hardness and standard deviation of the samples are presented in Fig. 3.2. The result of this analysis is particularly interesting since very rapid curing is observed during the first hour. It was initially thought that a linear curing rate would be obtained; however, the outcome more closely resembles an exponential curve. Interfacial chemical adhesion between the polyurethane and FRP composite pipe requires that the liner be in a partly cured state. Using Fig. 3.2 as a guideline, the hardness percentage of the liner can be estimated; it is assumed that this value is indicative of: (a) the cure state and, (b) the remaining available isocyanate groups within the semi set urethane.

3.3 Experimental

3.3.1 Sample Fabrication

Fabrication of the prototype pipe specimens can be segmented into three stages: (a) liner fabrication, (b) filament winding, and (c) curing. The following section details the above phases and places an emphasis on laboratory manufacturing procedures, however, the techniques implemented can potentially be scaled-up to meet industrial requirements; this aspect will be addressed in the discussion section.

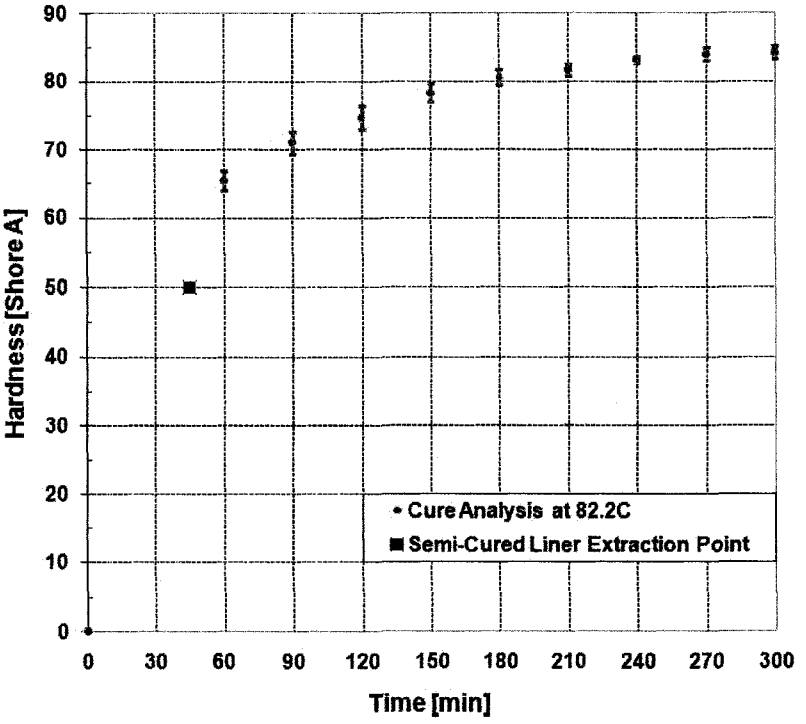

Figure 3.2: Polyurethane cure rate analysis

a. Liner Fabrication

Castable liquid NR-606M polyurethane was pneumatically injected into a preheated (82.2°C) aluminum mould that formed an annulus around a cylindrical steel mandrel. The setup was placed into a preheated oven (82.2°C). If the liner and the composite structure were to be mechanically bonded, the polyurethane was cured for 5 hours. However, to achieve a chemical bond the liner was cured for 45 minutes; this curing time endowed the urethane with sufficient rigidity such that it can be extracted from the mould without tearing, however, the liner had to be handled extremely delicately to avoid any damage during processing. Figure 3.2 illustrates the semi-cured liner extraction point; after 45 minutes of pre-curing, the liner had an average Shore A hardness of 50, which corresponded to a hardness percentage of approximately 60%. This value was obtained by dividing the semi-cured liner hardness by the hardness at full cure.

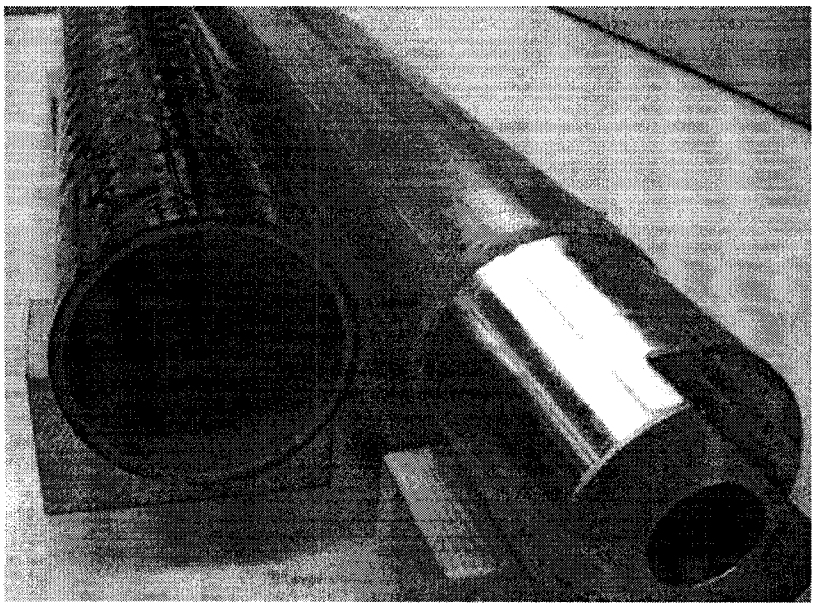

Figure 3.3: left) Completed pipe, right) Semi-cured polyurethane liner on a steel mandrel

Figure 3.3-right shows a partially cured polyurethane sleeve on a steel mandrel. It should be noted that for the prototype pipe, a liner thickness of 1.5875 mm (0.0625 in.) was selected; however, this value can be altered to suit pipeline conditions or manufacturing constraints.

b. Filament Winding

Following pre-curing of the liner, the polyurethane wrapped steel mandrel was positioned into the in-house industrial filament-winding machine. Tensioned basalt fiber tows were directed through an epoxy resin bath, and then helically wound onto the urethane liner in a $[\pm 60_2^\circ]$ fiber lay-up pattern. Similar to the liner thickness, the fiber architecture can be designed to meet pipeline strength requirements.

c. Curing

After winding was completed, the pipe structure was inserted into a fully automated oven for final curing. For the chemically bonded pipe specimens, it is during this

curing period that the polyurethane and the epoxy were able to form an interfacial bond. The curing procedure involved heating the specimen to 80°C for one hour; this was followed by increasing the temperature to 120°C for two-and-half hours. Figure 3.3-left illustrates the prototype pipe after mandrel extraction and machining.

3.3.2 Testing Procedure

A MTS testing machine was utilized in this investigation. To facilitate mounting of the pipe into the apparatus, aluminum tabs were adhesively bonded to each end of the specimen. A strain gauge rosette, positioned in the axial and hoop directions, was fastened on the outer surface of the pipe. Once installed in the testing machine, specimens were subjected to internal pressurization while maintaining a constant hoop-to-axial stress ratio of [2H:1A] with a 6.89 kPa/s (1 psi/s) monotonic loading rate, this type of test is also referred to as an unrestrained pressure test since the ends of the pipe are free to move axially during loading. The machine's data acquisition system recorded internal pressure, strain gauge data and intensifier volume.

In this preliminary experimental investigation, one unlined, and four lined basalt fiber-reinforced composite pipe were tested. Specimen characteristics are summarized in Table 3.1.

Table 3.1: Specimen characteristics

Specimen No.	**KJ229**	**KJ249**	**KJ269**	**KJ226**	**KJ267**
Bond Type	unlined	chem.	chem.	mech.	mech.
Liner Thickness (mm)	—	1.5875	1.5875	1.5875	1.5875
Comp. Wall Thickness (mm)	0.949	0.949	0.949	0.949	0.949
Inside Diam. incl. Liner (mm)	50.8	50.8	50.8	50.8	50.8
Inside Diam. excl. Liner (mm)	50.8	53.975	53.975	53.975	53.975
Gauge Length (mm)	254	177.8	254	254	254

3.4 Results

Stresses in the composite pipe wall were computed using Equations 3.1 and 3.2 [4]:

$$\sigma_{\text{hoop}} = \frac{ID(P_{\text{i}} - P_{\text{o}}) - 2tP_{\text{o}}}{2t} \tag{3.1}$$

$$\sigma_{\text{axial}} = \frac{ID(P_{\text{i}} - P_{\text{o}}) - 4P_{\text{o}}(ID + t)t}{4(ID + t)t} + \frac{F_{\text{A}}}{\pi(ID + t)t} \tag{3.2}$$

where,

P_i=Internal Pressure

P_o=Atmospheric Pressure

ID=Internal Diameter

t=Wall Thickness

F_A=Applied Axial Load

Under [2H:1A] loading conditions, which is commonly referred to as pressure vessel loading, there is no applied axial force, thus F_A=0. The wall thickness was determined using an analytical method described in [4], which requires calculation of the specimen's fiber volume fraction. This procedure required machining the outer surface of a 25.4 mm ring sample to remove the resin rich layer (since it does not contribute to structural strength). The specimen was placed into a 540°C oven to burn off the epoxy resin leaving only the basalt fibers behind. By measuring the weight before and after the burn-off process, the fiber volume fraction was determined. It should be noted that the specimens in this paper were not machined, however, the result of the fiber volume fraction and wall thickness are in excellent accordance with samples that did not include the resin rich layer. Furthermore, since: (a) using a burnout test to accurately determine the fiber volume fraction of a polyurethane lined ring sample is not possible, and (b) acid digestion testing is not readily available, it is assumed

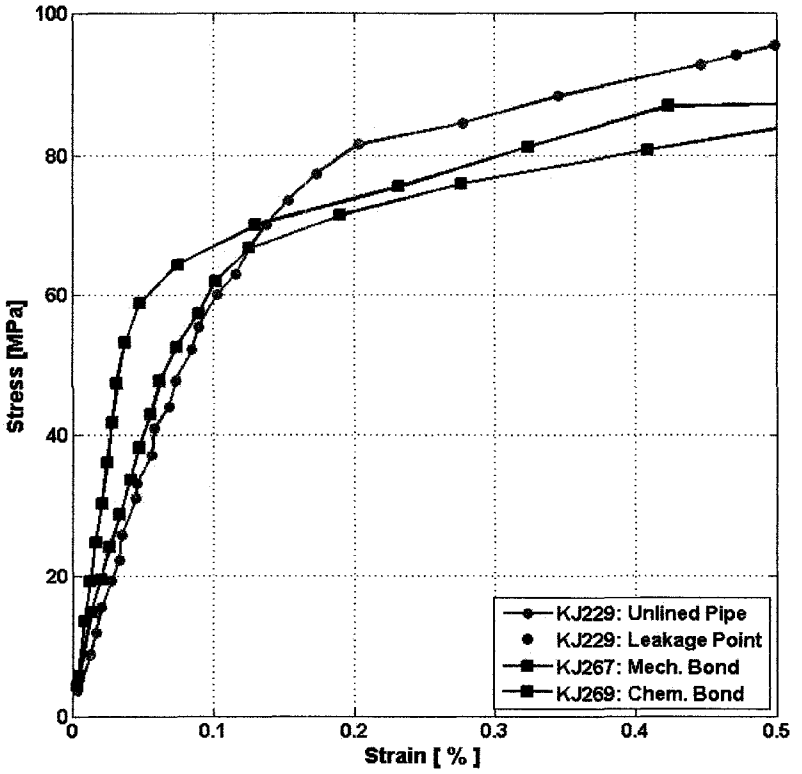

Figure 3.4: Axial stress-strain curve for [2H:1A] loading

that the fiber volume fraction (59.2%) and wall thickness (0.949 mm) of the unlined pipe (KJ229) was equivalent to that of the lined pipes. The slightly larger inside diameter of the lined pipe would have only a negligible effect on the fiber volume fraction and wall thickness, therefore the above statement is valid. It should be noted that the stress is calculated only in the compoiste structure and the liner thickness is negelected, the values for the inner diameter excluding the liner thickness are given in Table 3.1. Figures 3.4 and 3.5 show typical axial and hoop stress-strain curves for the specimens, respectively.

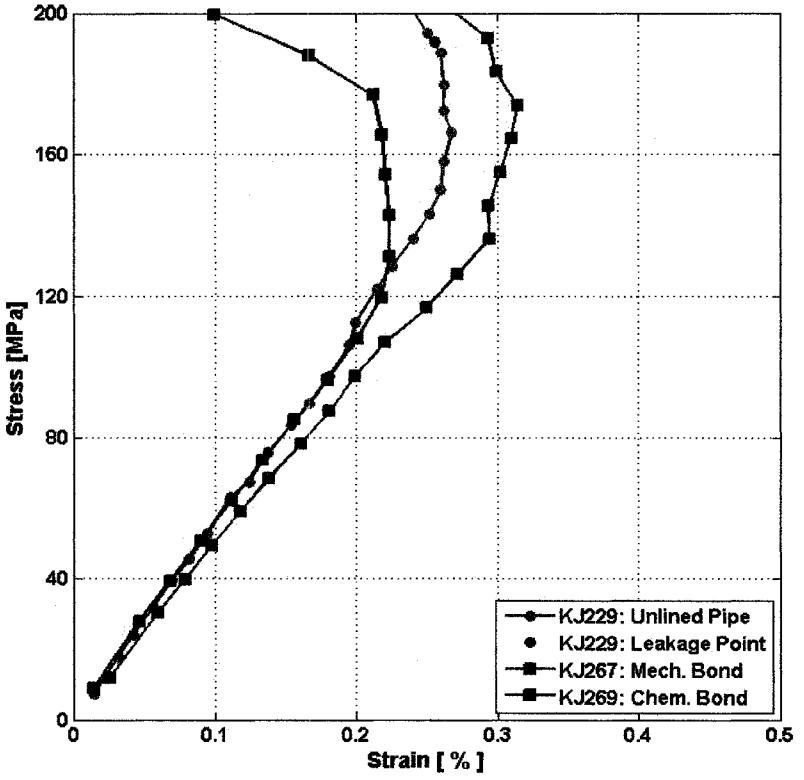

Figure 3.5: Hoop stress-strain curve [2H:1A] loading

Figure 3.6 illustrates the typical leakage of the unlined composite pipe. Volumetric data recorded from the MTS intensifier, which has been adjusted for expansion and compression of the specimen and the testing machine's hydraulic lines, can be utilized to determine the onset of weepage in the pipe [5]. The leakage threshold was achieved once the pipe lost 1% of its internal fluid.

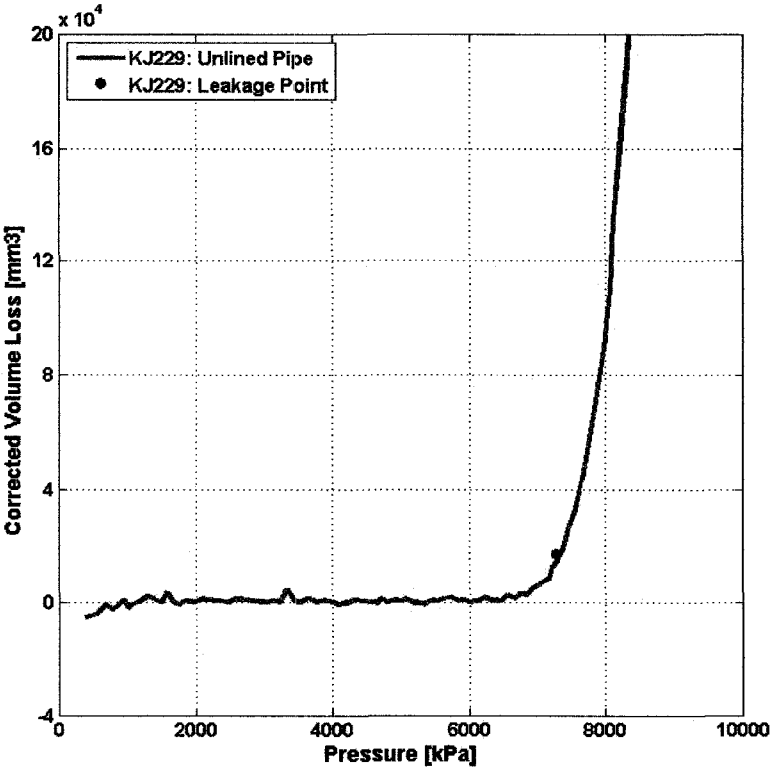

Figure 3.6: Leakage curve for unlined FRPC Pipe

3.5 Discussion

In this investigation, two distinct failure modes of: (a) weepage, and (b) burst were observed. The polyurethane lined pipes failed under burst failure due to fiber-fracture, which occurred at an average internal pressure of approximately 9.83 MPa (8.76 and 10.9 MPa) for mechanically bonded specimens and 13.23 MPa (12.7 and 13.74 MPa) for chemically bonded samples. Based on this preliminary analysis, the results indicate that a chemically bonded PU-composite pipe interface may delay the onset of burst failure relative to its mechanically bonded counterpart. It is theorized that the polyurea compound created at the interface during chemical bonding helps distribute the stress uniformly in the composite pipe, thus minimizing the impact of localized

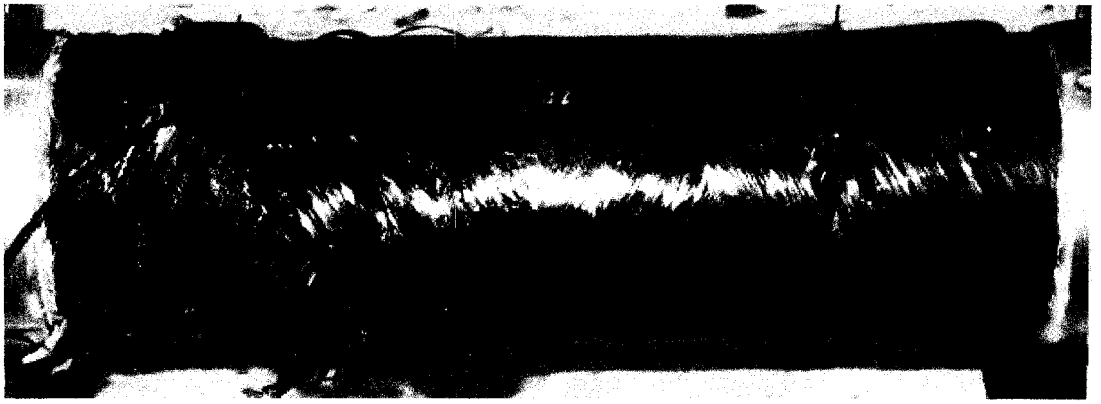

Figure 3.7: Burst failure of the polyurethane lined FRPC pipe under [2H:1A] loading

stress concentrations caused by micro-cracks in the epoxy matrix and thereby delaying the onset of fiber fracture. Figure 3.7 illustrates the typical catastrophic structural damage that occurs during burst failure. As expected, the unlined FRP tubular underwent functional leakage failure, and experienced weepage at an internal pressure of approximately 7.27 MPa. Table 3.2 summarizes the results of the preliminary pipe testing investigation.

Table 3.2: Preliminary pipe testing results

Specimen No.	**KJ229**	**KJ249**	**KJ269**	**KJ226**	**KJ267**
Bond Type	unlined	chem.	chem.	mech.	mech.
Failure Pressure (MPa)	7.27	13.74	12.7	8.76	10.9
Failure Type	Weepage	Burst	Burst	Burst	Burst

The pronounced curvature in the hoop stress-strain curves occurs due to fiber realignment during [2H:1A] loading. Note that under [2H:1A] loading only a $\pm 55^{\circ}$ fiber layup is able to resist the forces resulting from pressurization by pure tension in the filaments. Hence, as the epoxy matrix breaks down, the fibers, which are wound $\pm 60^{\circ}$ to the axial plane, tend to shift into the preferred direction causing

decreased hoop and increased axial strain. It is interesting to note that the strain for a given stress level in the chemically bonded pipe is half than that of the unlined and mechanically bonded specimens. This may be caused by: (1) a damaged or misaligned hoop strain gauge, or (2) non-uniform strain distribution in the composite structure. Although there is potential for the first case to occur, recent unpublished experimental work within the author's research group has shown preliminary evidence that surface strain in filament-wound composite tubulars is non-uniform, therefore the gauge may have been placed in a location with low local strain.

The shifting of fibers in the unlined pipe roughly corresponds to the initiation of leakage; this indicates that functional weepage failure is dominated by matrix degradation. Hence, a pipe commissioning process that loads a lined FRP pipe to the corresponding internal pressure associated with the aforementioned fiber-shifting phenomenon may provide the necessary micro-matrix cracks required for adequate venting of trapped interfacial volatiles. Although this procedure is promising, additional research is required to quantify the uniformity of matrix cracking over the pipe's surface.

Although there is potential for industrial application, further research is required to assess the interfacial bonding strength between the polyurethane and epoxy. Performing experimental fracture tests on urethane-epoxy samples formed in a similar fashion as the pipe specimens will provide a measure of bond toughness and will refine the pipe manufacturing methodology by highlighting the influence of bond type (mechanical vs. chemical) on interfacial strength. Moreover, it is also necessary to analyze the performance of lined FPC pipe after long-term exposure to a hydrocarbon rich environment; this is important to quantify the lifespan of the piping system.

3.6 Conclusion

This study presented a novel internally lined fiber-reinforced composite pipe suitable for use in slurry transportation. Production of the prototype involved filament winding epoxy impregnated basalt fibers onto a polyurethane liner. The purpose of this study was to: (a) describe the above laboratory based fabrication procedure, and (b) to present results of a preliminary experimental investigation. The experimental analysis compared the failure behaviour of unlined to lined FPC composite tubulars subjected to a constant biaxial loading ratio of [2H:1A]. The results showed that the unlined pipe experienced weepage failure at an internal pressure of 7.27 MPa, whereas the polyurethane lined pipe exhibited catastrophic burst failure which occurred at an average internal pressure of approximately 9.83 MPa for mechanically bonded specimens and 13.23 MPa for chemically bonded samples. Furthermore, the results illustrated that interfacial bond type did affect the burst strength of the lined composite pipes. As part of a comprehensive study on the development of a continuous and cost-effective lined composite piping system, future work should involve:

- Quantifying the uniformity of micro-matrix cracks introduced during the pipe commissioning process
- Investigating the interfacial bond strength through experimental fracture mechanics
- Analysis of pipe integrity after long-term exposure to hydrocarbons

Bibliography

[1] Mertiny, P., Ellyin, F., Hothan, A., "An experimental investigation on the effect of multi-angle filament winding on the strength of tubular composite structures," Composites Science and Technology, vol. 64, pp. 1-9, 2004.

[2] Wu, S., "Polymer interface and adhesion," New York: Marcel Dekker, pp. 406, 1982.

[3] Petrie, E., "Handbook of adhesives and sealants, 2nd Edition," McGraw Hill, pp. 161-166, 2000.

[4] Mertiny, P., Ellyin, F., "Influence of the filament winding tension on physical and mechanical properties of reinforced composites," Composites: Part A, vol. 33, pp. 1615-1622, 2002.

[5] Mertiny, P., Gold, A., "Quantification of leakage damage in high-pressure fiber-reinforced polymer composite tubular vessels," Polymer Testing, vol. 26, pp. 172-179, 2007.

Chapter 4

Polyurethane-Epoxy Interface Adhesion: An Experimental Investigation

4.1 Introduction

In the previous chapter, an internally lined fiber-reinforced polymeric composite piping solution was outlined. Manufacturing of the small-scale tubular is centered on filament-winding epoxy impregnated basalt fibers onto a polyurethane liner. If the liner is fully cured prior to the filament winding session, the PU and composite pipe form a mechanical bond. Conversely, if the polyurethane is only partially cured prior to filament winding, the liner and composite pipe are capable of forming a chemically bonded interface through the reaction of isocyanate in the semi-cured polyurethane and the amine curative agent in the epoxy resin. Chemically bonding the liner and the composite pipe has the advantage of establishing a strong interfacial bond; however, since the polyurethane is in a partly cured state it is prone to ripping and cleaving during production. Cleaving is not seen in fully cured liners, therefore they do not

need to be handled delicately.

Optimization of the above prototype pipe manufacturing process must ultimately satisfy the following question: Does the strength of the chemical bond justify the added difficulty of using a semi-cured liner? Currently, the strength of the mechanically bonded and chemically bonded PU-epoxy interfaces is unknown; therefore the objective of this study is to investigate the influence of interfacial bond type on adhesive fracture strength in order to optimize the PU lined composite pipe production protocols. To elucidate the aim of this chapter, an experimental fracture mechanics approach will be utilized to establish the toughness of chemically bonded and mechanically bonded polyurethane-epoxy interfaces. As such, this section will: (a) review suitable fracture mechanics literature, (b) describe sample fabrication, experimental setup and testing procedures, and (c) present results of the investigation.

4.2 Theory

There are a variety of experimental methods such as the double cantilever beam test, wedge test and lap shear test which are available for measuring interfacial toughness. However, the peel test is the most frequently used approach to determine the interfacial fracture strength between flexible elastomers and rigid substrates. Despite the relative ease of performing the experimental peel technique, it has been found that a true measure of the fracture energy is difficult to obtain from test data because most of the applied energy is dispersed or stored in deforming the sample rather than propagating the actual fracture process [1].

A lesser known option to the peel test is the pressurized blister test, which was originally proposed by Danneberg in 1961 [2]. This experimental fracture technique (see Figure 4.1) centers on injecting pressurized fluid through a circular hole in the substrate as a means of causing the elastomeric overlayer to blister, and eventually

debond from the rigid substrate. By measuring the maximum blister height (H), pressure (P), and debond radius (a) during crack growth the interfacial adhesion energy (Γ) can be readily determined.

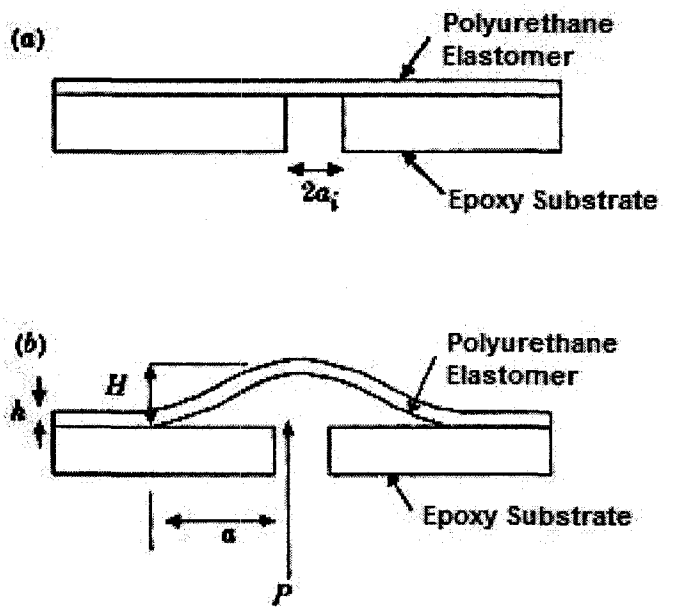

Figure 4.1: a) Blister specimen before pressurization, b) Blister specimen after pressurization (adopted from [3])

In comparison to the peel test, there are several main advantages of the blister test [1]: (a) there is no physical attachment or contact with the immediate test area, (b) both the loading process and debonding surface are axis-symmetric, and (c) the rate and angle of detachment are comparatively low. To achieve accurate results using blister test data, it is imperative that the proper principal mode of deformation is selected. The deformation mode of the blister test is governed by the ratio of $\frac{h}{a}$ (or overlayer thickness to the initial debond radius). As such, there are three possible regimes for the blister test [4]:

1. infinite medium solution: the overlayer thickness is much larger than the initial debond radius;

2. bending solution: the overlayer thickness is comparable to the initial debond radius; and

3. membrane solution: the overlayer thickness is much smaller than the initial debond radius.

According to [3] if $\frac{h}{a}$ >5 the infinite medium solution proposed by Williams in [5] is suitable for determining the interfacial fracture strength. When 0< $\frac{h}{a}$ <5 there are two methods to calculate the stored elastic strain energy, and depend on whether bending or membrane stretching is selected as the dominate deformation mode. It is stated in [3] that if $\frac{h}{a}$ <3, then the mode of deformation is encompassed within the membrane solution range; however Takashi and Yamazaki [6] suggest that the transition to a membrane solution occurs when $\frac{h}{a}$ <0.55. The present investigation utilizes a $\frac{h}{a}$ value of approximately 0.27, therefore the data analysis falls within the membrane solution domain proposed in [3] and [6]. Furthermore, it should be noted that the current blister test arrangement is centered on a exceedingly extensible polyurethane overlayer, thus, it is reasonable to assume that a fracture energy calculation based on an elastic stretching analysis would be more accurate than an analysis formed on a bending dominated premise [3].

Table 4.1: Equations available for determining fracture strength based on experimental blister data (adopted from [3])

Author	**Reference**	**Equation**	**Model Type**
Takashi and Yamazaki	[6]	$\Gamma = \left[\frac{P_c^4 a^4}{18.2Eh}\right]^{\frac{1}{3}}$	Membrane
Gent and Lewandowski	[4]		
a) Radius		$\Gamma = \left[\frac{P_c^4 a^4}{17.4Eh}\right]^{\frac{1}{3}}$	Membrane
b) Height		$\Gamma = 0.649 P_c H_c$	Membrane
Briscoe and Panesar	[3]	$\Gamma = \left[\frac{P_c^4 a^4}{576Eh(1-\nu)^2}\right]^{\frac{1}{3}}$	Membrane

From Table 4.1, it is evident that there are several membrane formulations available to calculate the interfacial fracture toughness from experimental blister test data. The formulas given by Taskashi and Yamazaki, Gent and Lewandowski (formula a) and Briscoe and Panesar require computation of the debond radius, a, at the critical pressure, P_c; however, determining the instantaneous debond radius requires the use of a high-speed and high-resolution camera to capture images of the blister as it is pressurized. As such, it is an expensive method in terms of equipment costs, calibration and data processing. Conversely, equation b given by Gent and Lewandowski, which is centered on Griffith's energy balance criterion, provides a relation between the fracture strength, critical pressure (P_c), and blister height (H_c) at the critical pressure. The P_c is defined at the apex of the pressure-maximum blister height curve [4]; thus, by determining the blister height corresponding to the critical pressure, the fracture strength of a can be readily established. This governing equation has two main advantages over the previously discussed formulas: (1) it is free of the overlayer's material properties, such as Young's modulus and Poisson's ratio, (2) it is significantly easier to measure the height of the blister than it is to determine the debond radius using a camera. The blister height can be captured and easily integrated into the data acquisition system using a linear variable displacement transducer (LVDT)–a similar height measuring technique was utilized by Liechti et al. [7]. Based on these benefits, this formulation will be utilized for data analysis within this chapter. For brevity, the derivation of this equation has been omitted; however, one can find the extensive mathematical formulation in the appendices of [4] and [8]. The major assumptions of this analysis include: (a) the material remains linearly elastic, (b) residual stresses are ignored, and (c) the analysis is purely mode I [4,8].

4.3 Experimental

4.3.1 Sample Fabrication

Fabrication of the blister test specimens is a two step process, and can be outlined as follows: (a) injection moulding the overlayer, and (b) casting the substrate onto the overlayer. The dimensions of the samples are outlined in Figure 4.2 and Table 4.2.

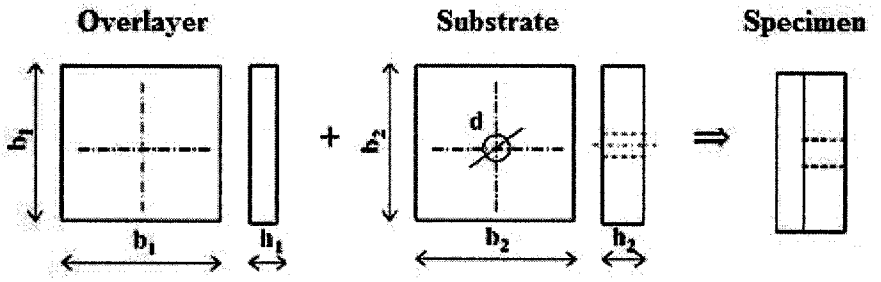

Figure 4.2: Blister specimen schematic (adopted from [9])

Table 4.2: Blister specimen dimensions

	Overlayer	Substrate
Material	Polyurethane (NR-606M)	Epoxy (EPON826-EPICURE9551)
b_1 (mm)	101.6	—
h_1 (mm)	2	—
b_2 (mm)	—	101.6
h_2 (mm)	—	5
d (mm)	—	15

a. Moulding the Overlayer

During step one, liquid polyurethane was injected into an aluminum mould, which had been pre-heated to approximately 82.2°C, immediately following the injection process, the mould was placed into a curing oven also pre-heated to 82.2°C. The amount of time the mould spent in the curing oven was dependent on whether the specimen was to be: (a) mechanically bonded, or (b) chemically bonded. If the blister specimen was to be mechanically bonded, the polyurethane overlayer was heated for 5 hours, allowing all the isocyanate functional groups to be consumed and thus fully cured. If the blister specimen was to be chemically bonded, the polyurethane overlayer was cured for 45 minutes, which roughly corresponds to a 60% hardness percentage, according to the cure-rate analysis performed in the preceeding chapter.

b. Casting the Substrate onto the Overlayer

After the overlayer had been appropriately cured, the mould was disassembled, and a new mould was fashioned around the polyurethane sheet. Using the new mould, the two part liquid epoxy resin was then cast onto the polyurethane, thus forming the substrate. It should be noted that a removable poly(tetrafluoroethylene) (PTFE) pin was used to create the central perforation required for pressurization of the blister.

The mould was subsequently placed into an oven to cure the epoxy and initially heated to 80°C for 60 minutes. This was then followed by further curing at 120°C for 150 minutes. For chemically bonded samples, it was during this phase that isocyanate within the partially-cured polyurethane reacted with polyamine groups within the epoxy resin curing agent, EPICURE9551, to create a polyurea compound at the interface.

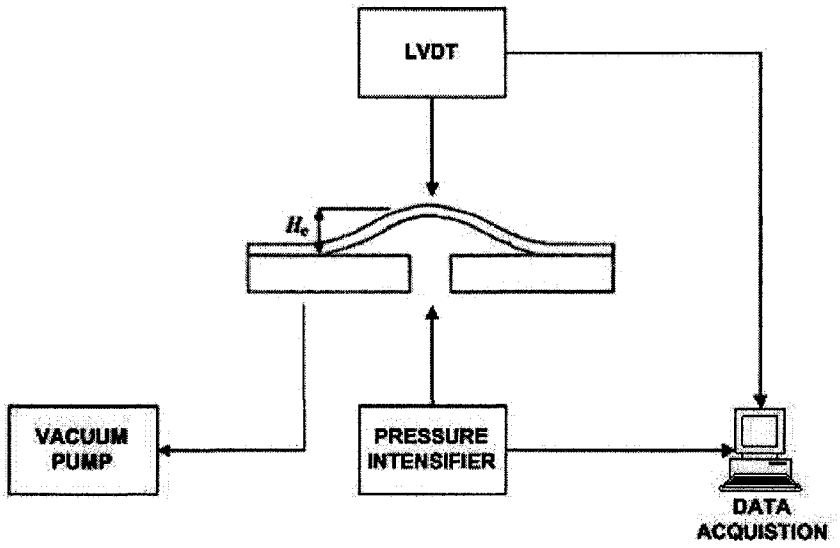

Figure 4.3: Schematic of the experimental setup

4.3.2 Experimental Setup and Testing Procedure

Figure 4.3 illustrates a schematic of the experimental test setup utilized in this investigation. To perform the blister experiments, specimens were placed onto the testing jig shown in 4.4. The specimens were secured to the fixture using a vacuum seal created between the inner and outer o-rings. It should be noted that the central perforation shown in Figure 4.2 was aligned with the fluid injection port, which allowed pressurized hydraulic oil (flow rate of 0.0159 ml/second) to inflate the blister. During the experiment, as the blister formed and increased in size, a sensitive linear variable displacement transducer captured the changing height. Additionally, data from the pressure intensifier and LVDT were digitally recorded at intervals of 0.3 seconds.

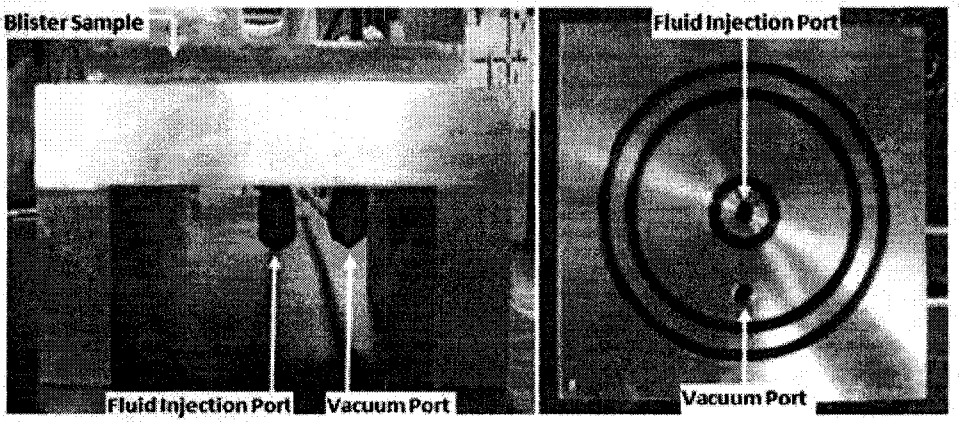

Figure 4.4: Experimental blister testing jig

4.4 Results and Discussion

In this investigation, two mechanically and three chemically bonded blister specimens were tested. Typical experimental relations between inflation pressure and maximum blister height for each bond type are shown in Figure 4.5.

In the case of the mechanically bonded specimens, as the membrane was inflated, the height of the blister also increased, but no change in the radius of the blister was visually detected. Once the critical pressure was achieved, interfacial fracture occurred causing a decrease in pressure. As mentioned previously, the critical pressure is defined at the apex of the Pressure-Maximum Blister Height curve; thus, by determining the blister height corresponding to the critical pressure, the fracture strength of a mechanically bonded PU-epoxy interface was established using Gent and Lewandowski's height formulation found in Table 4.1. Based on the two initial experiments, the average fracture toughness of the mechanically joined specimens was 1173.5 J/m^2 (1063 and 1284 J/m^2). For comparison, the adhesion strength of PU-steel blister specimens was found to be up to 457 J/m^2 [3]. Furthermore, the peel strength between poly(ethylene terephtalate)-epoxy and poly(ethylene terephtalate)-

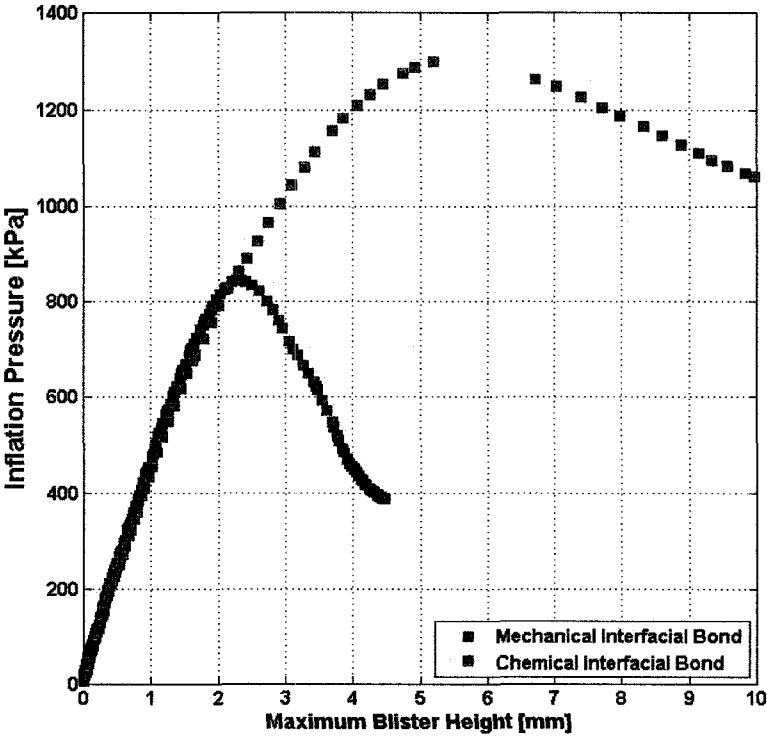

Figure 4.5: Typical experimental relations between pressure and max. blister height

PU was determined to be approximately 1600 J/m^2 and 1500 J/m^2, respectively [10]. which places the results of this preliminary analysis within correct range of values.

Conversely, the chemically bonded specimen did not exhibit interfacial fracture; based on a visual inspection during the experimental investigation, it was observed that as the membrane was pressurized the blister continued to grow in height, but not in radius. Subsequent pressurization led to permanant deformation of the polyurethane overlayer, in which the blister transformed into a balloon-like shape which is illustrated in Figure 4.6b. It is suspected that the change in blister shape leads to an increase in area, thus replicating the drop in pressure seen during interfacial fracture of the mechanically bonded specimens. It should be noted that the experiments were terminated to prevent the blister from rupturing. Post-experimental analysis of the chemically bonded samples showed significant permanant deformation in the blister region and, more importantly, no debonding around the central perforation. These

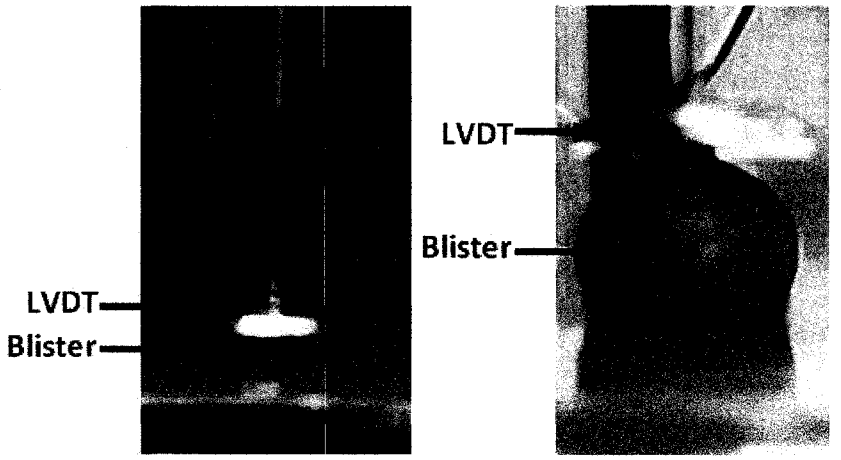

(a) Mechanically bonded specimen (b) Chemically bonded specimen

Figure 4.6: Comparison of blister size between interfacial bond type

observations suggest that the interfacial strength of chemically bonded PU-epoxy is greater than the ultimate strength of the polyurethane, and indirectly confirms that a new polyurea chemical compound is formed at the bond line. The constrained blister test is an alternative form of the blister test that allows for testing of strongly adherent overlayers [11], however, it is doubtful that fracture would occur even using this option due to the presence of the polyurea compound at the interface. The results of the preliminary blister testing are summarized in the following table.

Table 4.3: Preliminary blister testing results

Specimen No.	**B02**	**B03**	**B05**	**B06**	**B07**
Bond Type	mech.	mech.	chem.	chem.	chem.
Fracture Type	Interfacial	Interfacial	No Frac.	No Frac.	No Frac.
Fracture Strength (J/m^2)	1063	1284	—	—	—

Although only limited testing was performed, the results clearly demonstrate that chemically bonded polyurethane-epoxy interfaces are superior to their mechanically

bonded counterparts. In order to optimize the PU lined composite pipe production protocols for maximum interfacial toughness, it is suggested that chemical bonding be implemented.

4.5 Conclusion

This chapter investigated the toughness of mechanically and chemically bonded PU-epoxy interfaces through experimental fracture mechanics, via blister testing. By pressurizing the polyurethane overlayer through a central perforation and subsequently measuring the height and pressure of the blister at the instant interfacial fracture occurred the bond toughness could be evaluated. Through preliminary experiments, it was determined that mechanically bonded specimens had an average fracture strength of 1173.5 J/m^2. Conversely, it was observed that chemically bonded samples did not undergo interfacial fracture, instead extensive permanent deformation occurred in the blister region and tests were terminated to prevent the blister from rupturing. Based on these results it is recommended that chemical bonding be implemented over mechanically bonding in the pipe manufacturing process.

Bibliography

[1] Chu, Y.Z., Durning, C.J., "Application of the blister test to the study of polymer-polymer adhesion," Journal of Applied Polymer Science, vol. 45, pp. 1151-1164, 1992.

[2] Dannenberg, H., "Measurement of adhesion by a blister method," Journal of Applied Polymer Science, vol. 5, pp. 125-134, 1961.

[3] Briscoe, B.J., Panesar, S.S., "The application of the blister test to an elastomeric adhesive," The Royal Society Proceedings: Mathematical and Physical Sciences, vol. 433, no. 1887, pp.23-43, 1991.

[4] Gent, A.N., Lewandowski, L.H., "Blow-off pressures for adhering layers," Journal of Applied Polymer Science, vol. 33, pp. 1567-1577, 1987.

[5] Williams, M.L., "The continuum interpretation for fracture and adhesion," Journal of Applied Polymer Science, vol. 13, pp. 29-40, 1969.

[6] Takashi, M., Yamazaki, K., Natsume, T., Takebe, T., "Debonding of an Al-epoxy system by the blister method," Proceedings of The Japan Congress on Materials Research, pp. 260-264, 1978.

[7] Liechti, K.M., Hanson,E.C., "Nonlinear effects in mixed-mode interfacial delaminations," International Journal of Fracture, vol. 36, pp. 199-217, 1988.

[8] Shirani, A. and Liechti, K. M., "A calibrated fracture process zone model for thin film blistering," International Journal of Fracture, vol. 93, pp. 281-314, 1998.

[9] Figiel, L., Lauke, B., "Interface fracture of polymer films: blister test experiments and modelling," International Journal of Fracture, vol. 139, pp. 77-89, 2006.

[10] Wu, S., "Polymer interface and adhesion," New York: Marcel Dekker, pp. 398, 1982.

[11] Chang, Y-S., Lai, Y-H, Dillard, D.A., "The constrained blister: a nearly constant strain energy release rate test for adhesives," Journal of Adhesion, vol. 27, pp. 197211, 1989.

Chapter 5

Polyurethane-Epoxy Interface Adhesion: A Finite Element Analysis

5.1 Introduction

Failure mode and effects analysis (FMEA) is a risk analysis tool which can be utilized to identify and help mitigate potential material and equipment failures [1]. During risk assessments, finite element analysis is often used to understand the design limitations by helping to predict product behavior under the worst case scenario. Such an approach helps to reduce liability and ensures product safety and reliability. In the previous sections it was established that a chemically bonded polyurethane-epoxy interface was superior to a mechanically bonded interface, and should thus be implemented in the pipe fabrication methodology. However, using a risk assessment approach, future finite element analysis of the pipe should be centered on a model which is mechanically bonded as a means of determining design limitations. The objective of this chapter is to develop a finite element model to simulate crack initiation

based on the experimental fracture results of mechanically bonded blister specimens. It is anticipated that this parametric-based simulation will provide numerically calibrated interfacial strength parameters that can ultimately be implemented into future full-scale finite element analysis of the pipe. As such, this section will: (a) review relevant numerical fracture modeling techniques, (b) describe the finite element implementation, and (c) present results of the numerical investigation.

5.2 Numerical Fracture Mechanics Theories

According to [2], in numerical modeling of fracture processes there are two broad groups of analysis: (1) predictive based, and (2) simulation based. The first group of techniques usually rely on methods such as virtual crack closure to forecast the critical energy release rate. Conversely, the second class of techniques aim to replicate crack initiation based on experimentally established values for the critical energy release rate through the use of damage mechanics processes, such as cohesive zone models (CZM). Since the aim of this section is to simulate crack initiation of mechanically bonded PU-epoxy blister specimens based on experimentally established fracture parameters, the literature review will be dedicated to cohesive zone fracture modeling.

Cohesive zone modeling was first introduced in the late 1950s and early 1960s by Barrenblatt [3,4] and Dugdale [5], and over the last 40 years CMZs have been extensively utilized to simulate fracture in metals, ceramics, polymers, fiber composites and bimaterial systems [6]. The underlying assumption is that the cohesive zone finite elements, which are placed along the expected crack growth path, can simulate the fracture failure process through a defined normal and shear traction-displacement law that governs how the element will separate under loading. There are many cohesive zone models [3,5,7,8]; however, the main difference among them is how traction-separation laws are derived. Generally speaking, most cohesive models

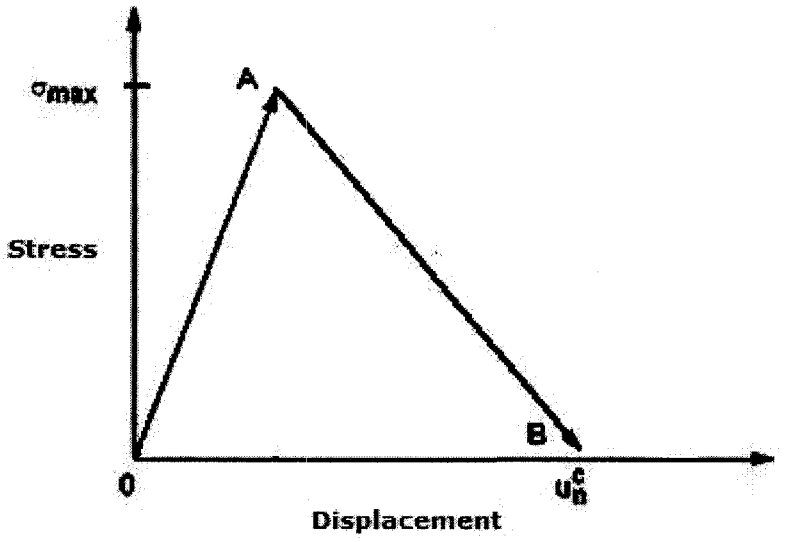

Figure 5.1: Bi-linear cohesive zone traction-separation model (adopted from [10])

specify that as interfacial separation (or displacement) occurs the traction will reach a maximum value, then decrease to allow complete debonding of the interface [6]. Furthermore, it was observed in [8] that results are not overly sensitive to the choice of separation law. Within ANSYS, there are two non-linear and iterative methods of performing interfacial delamination and failure simulations. The first technique incorporates interface elements with a built-in cohesive zone model, which are placed along the known path between the separating materials, while the second method incorporates contact elements with a built-in cohesive zone model at the interface of the two materials; both techniques use elements of zero thickness. Although these implementations are similar in nature, it should be noted that when utilizing the first method the constraints must be applied as boundary conditions since the use of forces and pressures will cause numerical instability due to rigid body motion after fracture occurs. This option is not feasible, as pressurization is the mode of loading in this study. Therefore, the contact element method based on the work of Alfano and Crisfield [9] is used to simulate crack initiation in the blister test. The bi-linear traction-separation used in the model is illustrated in Figure 5.1.

In Figure 5.1, $\overline{OA}$ represents the linear elastic loading path of the cohesive elements with debonding beginning at point A, while $\overline{AB}$ describes the linear softening which is initiated once the traction reaches the user defined value for the maximum cohesive tensile strength, $\sigma_{\max}$. Complete debonding is achieved at point C allowing the surfaces to separate. The area under the normal traction-separation curve is referred to as the cohesive separation energy and is considered to be the work of fracture, G_{cn}. For a mode I dominated problem, such as the one currently being investigated, the behaviour of the cohesive zone model can be described by relating the work of fracture, normal cohesive tensile strength and the critical normal displacement at complete debonding, $u_{\mathrm{c}}^{\mathrm{n}}$, through the following equation [11,12,13]:

$$G_{\mathrm{cn}} = \frac{1}{2}\sigma_{\max} u_{\mathrm{c}}^{\mathrm{n}} \tag{5.1}$$

Thus, by specifying values for the work of fracture and the maximum cohesive tensile strength the behaviour of the interfacial cohesive zone elements can be fully defined; thus, the values of G_{cn} and $\sigma_{\max}$ are considered the most important fracture parameters [11]. As mentioned above, the work of fracture can be determined from experiments, which was accomplished in the previous chapter and found to be 1173.5 J/m^2. However, the maximum cohesive tensile strength is a numerical parameter and must be selected through trial. As such, a parametric study will be undertaken to understand the influence of the G_{cn} and $\sigma_{\max}$ variables on the numerical blister model. Similar studies using the pressurized blister method to calibrate a cohesive zone model have concluded that a combination of experiments and finite element modeling are adequate for determining the cohesive zone parameters[11,12,13].

5.3 Finite Element Implementation

Based on the geometry of the problem, a two dimensional axis-symmetric finite element model was developed according to the dimensions of the blister specimen outlined in the previous chapter. Figure 5.2, which is not to scale, illustrates the overall concept. In the experimental tests, the blister specimens were fixed to the testing jig using a vacuum seal, while the overlayer was pressized via the central hole. To replicate these conditions in the finite element model, the bottom edge of the epoxy substrate is considered fixed in all degrees of freedom, while a uniform pressure loading is applied to the underside of the polyurethane strip.

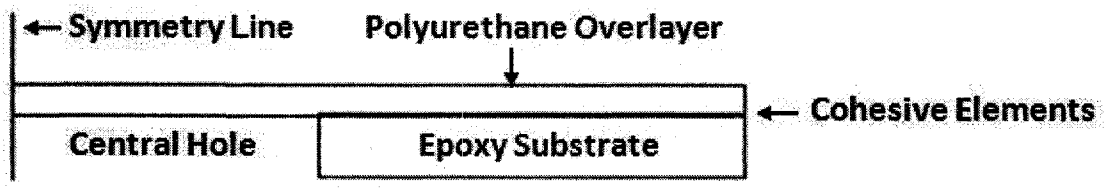

Figure 5.2: 2D Axis-symmetric model concept

From the uniaxial tensile test performed on the polyurethane, it is evident that the stress-strain behaviour is non-linear, and can be roughly approximated using a the two-parameter Mooney-Rivlin hyperelastic equation. Although hyperelasticity can be readily incorporated into the finite element model, it was found that the addition greatly increased computational time and led to convergence instabilities since the contact elements also require a non-linear iterative solution. To overcome this issue, the polyurethane and epoxy were both modeled as linearly elastic PLANE182 elements with Young's moduli of 21.5 MPa and 2.9 GPa, respectively, and Poisson's ratios of 0.44 and 0.42, respectively; the values for the epoxy were experimentally determined in [14] for the same resin system. The interfacial cohesive zone contact elements are based upon CONTA171-TARGE169 pairs.

In order to calibrate the finite element model to accurately predict the critical pressure (P_c) required for crack initiation, it is imperative that the influence of the interfacial cohesive zone properties are examined. To accomplish this, (a) σ_{max} was varied between 1.72, 2.15 and 2.58 MPa while G_{cn} was held constant at 1173.5 J/m^2, and (b) the cohesive separation energy was varied between 586.75, 1173.5 and 1760.25 J/m^2 while σ_{max} was held constant at 2.15 MPa. In the above two investigations the baseline case study is referred to as BASE and has cohesive zone properties of G_{cn}=1173.5 J/m^2 and σ_{max}=2.15 MPa. Following this analysis the parameters of the numerical model were selected to best fit the experimental blister test data obtained in the previous chapter (see Figure 4.5).

5.3.1 Model Reduction and Mesh Sensitivity Analysis

During preliminary finite element analysis it was observed that the outer portion of the model was not influenced by the pressurization of the polyurethane overlayer; thus, in an effort to further decrease computational time this region of the model was removed. This process leads to a direct reduction in computational time without influencing the results in the region of interest. Figure 5.3 shows the difference between the full scale model and reduced model.

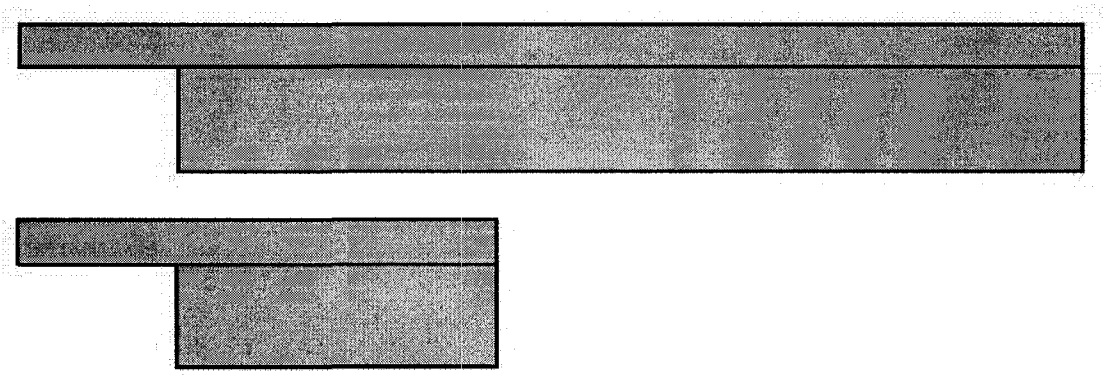

Figure 5.3: Comparison between full scale and reduced finite element models

Table 5.1: Mesh sensitivity analysis

Mesh Density	No. of Elements	Max. Deflection (mm)	CPU Time (s)
Low	580	1.696	11.938
Medium	1420	1.702	27.866
High	2160	1.702	42.891

To ensure that the reduced model was optimized for computational efficiency and numerical accuracy, an extensive mesh sensitivity analysis was performed. In this investigation the density of the elements was varied between low, medium and high to determine its influence on the maximum central displacement of the blister under an arbitrary uniform pressure loading of 500 kPa. For the mesh sensitivity numerical model, the cohesive zone parameters were selected to be G_{cn}=1173.5 J/m^2 and σ_{max}=25.1 MPa. Table 5.1 displays the results of the analysis.

The sensitivity investigation established that the medium density model, illustrated in Figure 5.4, provided results equivalent to that of the high density model, but with over 50% savings in computational time. Therefore, the medium density mesh was utilized in subsquent finite element analyses. It is important to note that the elements in the polyurethane overlayer are significantly smaller (ranging between 0.167 mm x 0.231 mm and 0.167 mm x 0.186 mm in size) than those found in the epoxy substrate (1 mm x 0.231 mm) since it is the region in which the deformation occurs.

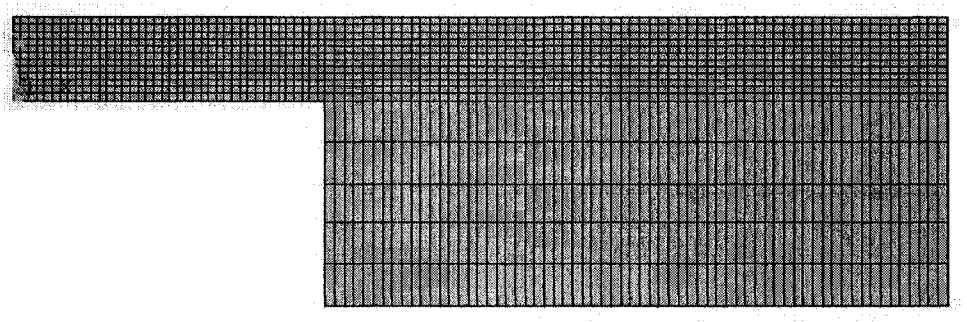

Figure 5.4: Medium density finite element mesh

5.4 Results and Discussion

5.4.1 Influence of Maximum Cohesive Tensile Strength

Figure 5.5 displays the effect of varying maximum cohesive tensile strength on the crack initiation in the finite element analysis, while holding the cohesive separation energy constant. Crack initiation in the model is seen as the abrupt change of the slope into a horizontal line; the x-y coordinates at this intersection are considered as the maximum blister height at debonding and the critical pressure required for debonding, respectively. Increasing σ_{max} by 0.43 MPa relative to the baseline case resulted in a 35 kPa increase in the critical pressure required for crack initiation; a decrease of the same amount in σ_{max} resulted in a 65 kPa decrease in the critical pressure required for crack initiation. It is evident that a slight change in the maximum cohesive tensile strength significantly influences the results, moreover, the relationship between σ_{max} and P_c is not linear in nature.

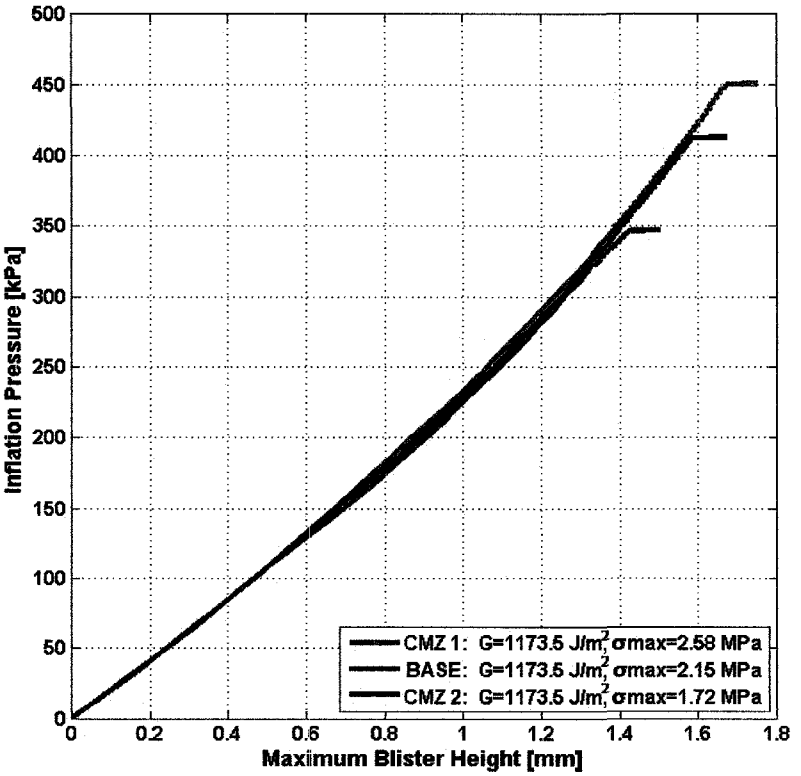

Figure 5.5: Variation of crack initiation pressure using a constant cohesive separation energy and variable cohesive tensile strength

5.4.2 Influence of Cohesive Separation Energy

Figure 5.6 depicts the effect of varying cohesive separation energy on the crack initiation in the finite element analysis, while holding the maximum cohesive tensile strength constant. It can be seen that considerable changes in the cohesive separation energy did not significantly influence the results, i.e. decreasing G_{cn} to 586.75 J/m^2 or 50% relative to the baseline case only decreased the critical pressure by approximately 20 kPa. This finding illustrates that the influence of the cohesive separation energy on the results is less important than that of the maximum cohesive tensile strength.

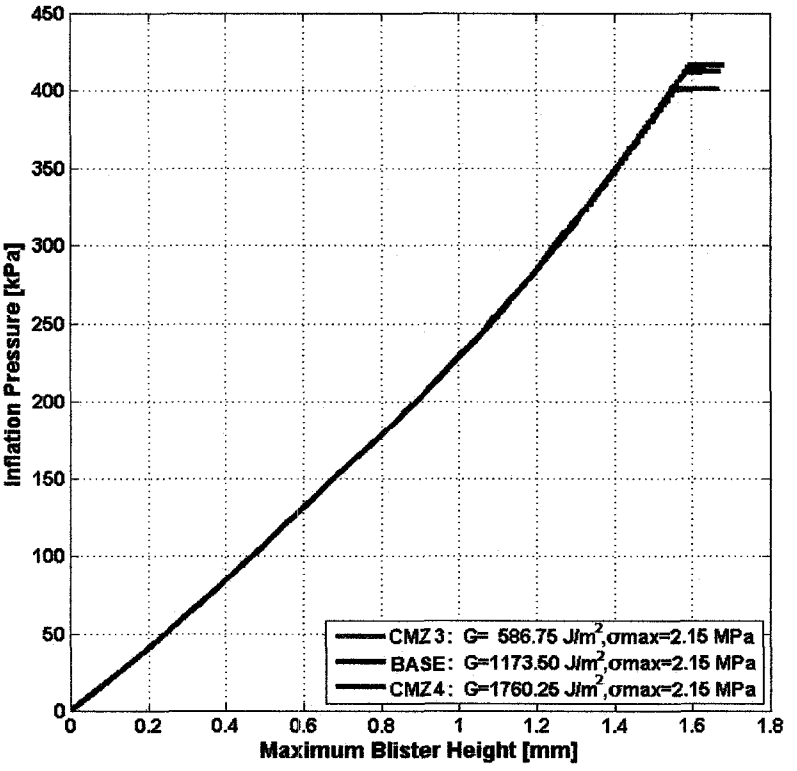

Figure 5.6: Variation of crack initiation pressure using a variable cohesive separation energy and a constant cohesive tensile strength

5.4.3 Comparison between Finite Element Model and Experimental Results

It was found that by implementing a cohesive separation energy of 1173.5 J/m^2, and a maximum cohesive tensile strength of 14.25 MPa the analysis was able to accurately predict the critical pressure required for debonding and the maximum central blister height. It is suggested that these coefficients, along with the previously outlined material properties, be implemented into future finite element analysis of the pipe. The results comparing the FEM analysis and experimental investigation can be found in Table 5.2. For reference, the ANSYS APDL code for this analysis is located in the Appendix.

Table 5.2: Comparison between experimental and FEM results. *From Figure 4.5.

	Exper. Results*	**FEM Results**
Critical Pressure	844 kPa	851 kPa
Maximum Blister Height	2.34 mm	2.25 mm

Figures 5.7, 5.8 and 5.9 show the crack initiation, von Mises stress and von Mises strain in the model utilized to simulate crack initiation of the mechanically bonded experimental blister specimen, respectively. As expected, the maximum von Mises stress is found around the crack tip region, with a value of 9.8 MPa, which indicates that localized plastic deformation has occurred (assuming 0.2% offset yield point to the tensile stress-strain curve in Figure 2.7). This argument is further supported by the von Mises strain distribution showing strains well above 40% in this location. However, the bulk of the polyurethane overlayer remains on the cusp of the linear stress-strain regime, thus validating the use of a linear eleastic material model. It is also interesting to note the significant difference in strain levels seen in the polyurethane and the epoxy substrate; this phenomenon occurs due to the extreme mismatch in elastic moduli between the material, and can be explained through Hooke's Law.

Future work should focus on further verification of the cohesive parameters. This can be accomplished by experimentally testing a blister specimen with a different PU overlayer thickness, and determining the corresponding critical pressure for crack initiation and maximum blister height at debonding. If the above determined CZM parameters are accurate, then they should be capable of accurately modelling the new blister geometry. In addition, a parametric study also analyze the error attributed to uncertainty in the modulus of elasticity and Poisson's ratio on the numerical results.

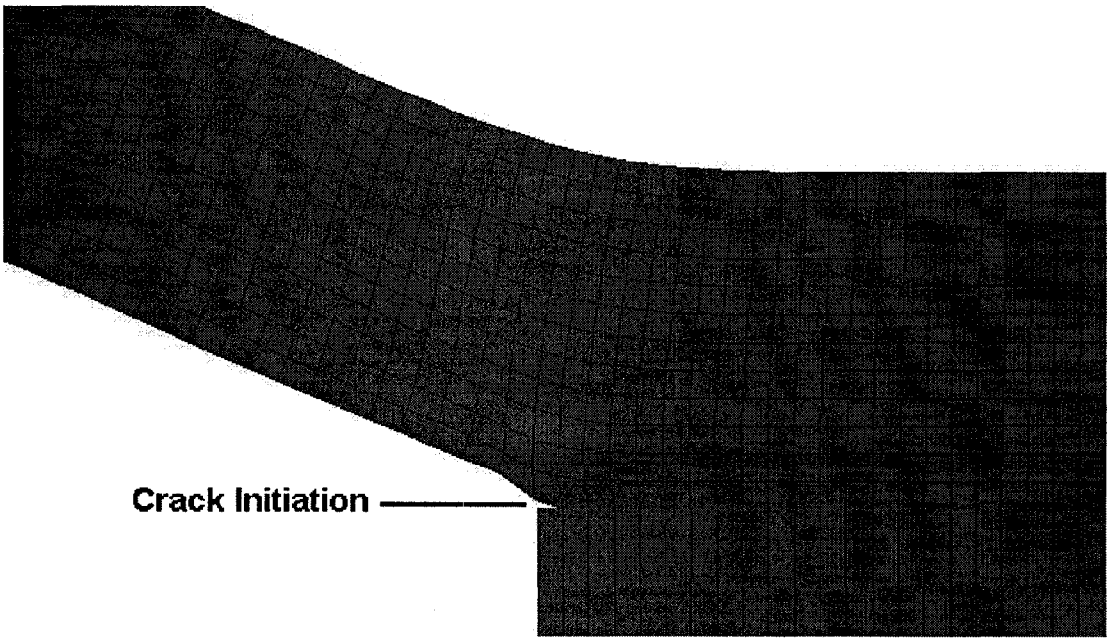

Figure 5.7: Crack initiation in the blister model

5.5 Conclusion

The aim of this chapter was to develop a finite element model to simulate the start of debonding based upon experimentally determined fracture results of mechanically bonded blister samples. A parametric analysis was performed on the cohesive zone parameters to elucidate their influence on the applied pressure required for crack initiation. This investigation determined that maximum cohesive tensile strength had a much greater effect than that of the cohesive separation energy. Next, the cohesive zone parameters were calibrated (G_{cn}=1173.5 J/m^2, σ_{max}=14.25 MPa) to match the experimentally established critical pressure for crack initiation. It is anticipated that these values can be readily incorporated into future finite element investigations that require modeling of a mechanically bonding polyurethane-epoxy interface subjected to mode I loading conditions.

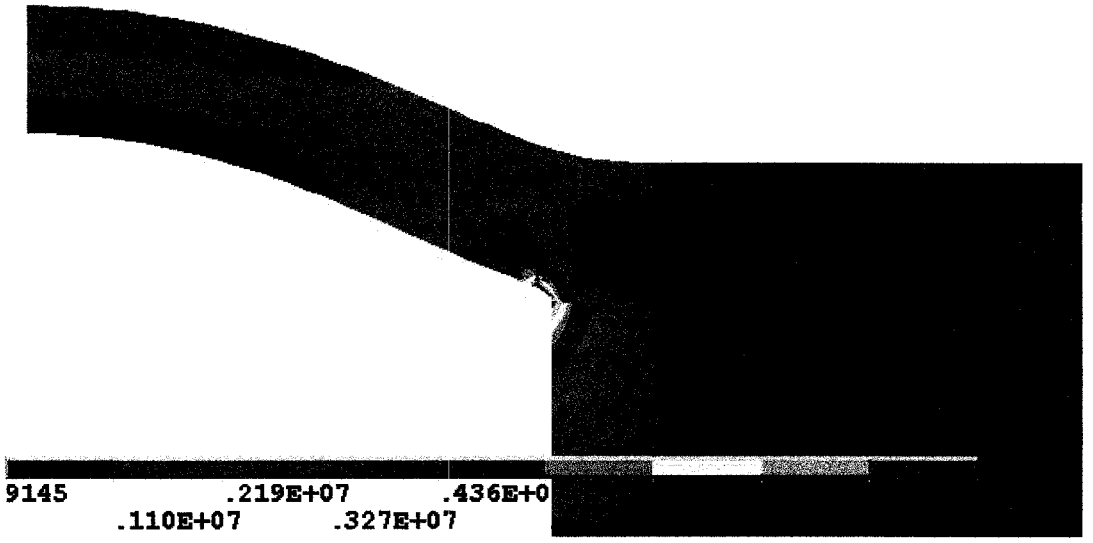

Figure 5.8: von Mises stress distribution in the blister model

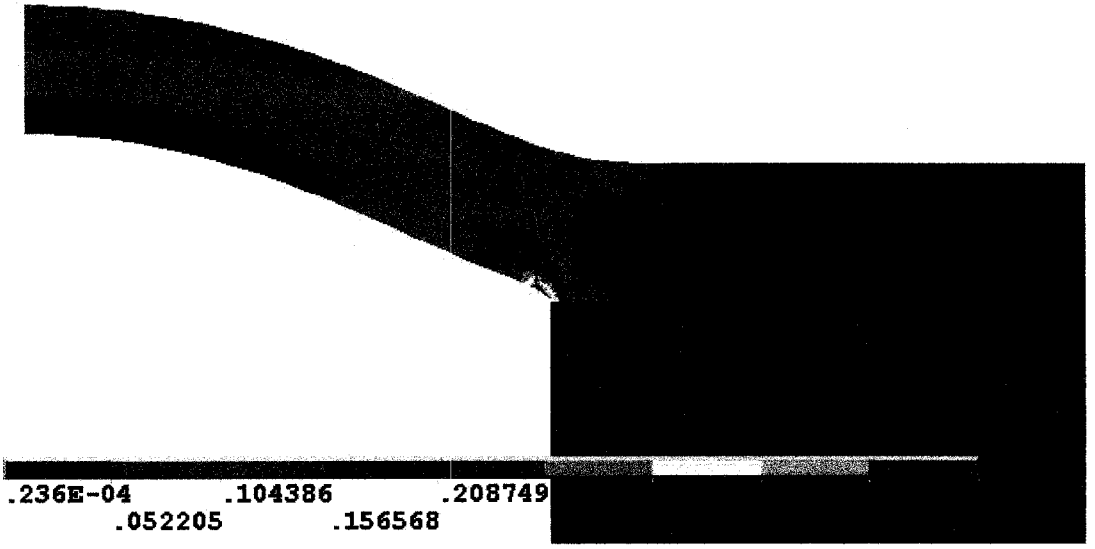

Figure 5.9: von Mises strain distribution in the blister model

Bibliography

[1] Daydem Engineering Corporation, "Guidelines for failure mode and effects analysis for automotive, aerospace and general manufacturing industries," Boca Raton, FL : CRC Press, 2003.

[2] Fan, C., Jar, P.-Y.B., Cheng, J.J.R., "Cohesive zone with continuum damage properties for simulation of delamination development in fibre composites and failure of adhesive joints," Engineering Fracture Mechanics, vol. 5, no. 13, pp. 3866-3880, 2008.

[3] Barenblatt, G.I., "On equilibrium cracks formed in brittle fracture: general concepts and hypotheses. Axis-symmetric cracks." Journal of Applied Mathematics and Mechanics, vol. 23, no. 3, pp. 622-636, 1959.

[4] Barenblatt, G.I., "The mathematical theory of equilibrium cracks in brittle fracture," Advances in Applied Mechanics, vol. 7, pp. 55-129, 1962.

[5] Dugdale,D.S., "Yielding of steel sheets containing slits," Journal of the Mechanics and Physics of Solids, vol. 8, pp. 100108, 1960.

[6] Shet, C., Chandra, N., "Analysis of energy balance when using cohesive zone models to simulate fracture processes," Transactions of the ASME: Journal of Engineering Materials and Technology, vol. 124, pp. 440-450, 2002.

[7] Needleman, A., "An analysis of decohesion along an imperfect interface," International Journal of Fracture, vol. 32, pp. 21-40, 1990.

[8] Tvergaard, V., Hutchinson, J.W., "On the toughness of ductile adhesive joints," Journal of the Mechanics and Physics of Solids, vol. 44, no. 5, pp. 789-800, 1996.

[9] Alfano, G. and Crisfield, M.A., "Finite element interface models for the delamination analysis of laminated composites: mechanical and computational issues," International Journal for Numerical Methods in Engineering, vol. 50, pp. 1701-1736, 2001.

[10] ANSYS Theory Manual. 11 ed. : ANSYS Inc., 2005.

[11] Shirani, A. and Liechti, K. M., "A calibrated fracture process zone model for thin film blistering," International Journal of Fracture, vol. 93, pp. 281-314, 1998.

[12] Hbaieb, K., Zhang, Y.W., "A parametric study of a pressurized blister test for an elastic plastic film-rigid substrate system," Material Science and Engineering A, vol. 390, pp. 385-392, 2005.

[13] Jiang, L.M., Zhou, Y.C., Liao, Y.G., Sun, C.Q., "A pressurized blister test model for the interface adhesion of dissimilar elastic-plastic materials," Material Science and Engineering A, vol. 487, pp. 228-234, 2008.

[14] Tao, G., "Multiaxial fatigue of an epoxy polymer: experiments and theories," University of Alberta: PhD Thesis, 2007.

Chapter 6

Conclusion and Summary

The objective of this thesis was to establish preliminary experimental and analytical framework for development of a novel small-scale polyurethane lined basalt fiber-reinforced epoxy impregnated composite tubular. This was accomplished through a four part paper series which addressed: a) testing of the polyurethane, b) fabrication and preliminary experimental testing of the piping system, c) optimization of the fabrication methodology through a fracture mechanics approach, and d) a finite element analysis to model interfacial crack initiation. The following summary will highlight important conclusions and results from each section.

a. Material Characterization: Polyurethane Elastomer Tensile Testing

Tensile testing was successfully performed on the polyurethane elastomer selected for the internal liner of the composite pipe. Specimens were formed according to the ASTM D638-03 standard, and tested at a constant axial extension rate of 50 mm/minute. The average Young's modulus and Poisson's ratio were determined to be 21.5 MPa and 0.44, respectively. Lastly, it was observed that of the two theoretical

models presented to describe the polyurethane's stress-strain behaviour, the two-parameter Mooney-Rivlin model was superior in depicting the overall shape.

b. Fabrication and Performance of a Polyurethane Lined Composite Pipe

A fabrication methodology was created to develop an internally lined fiber-reinforced composite pipe; the laboratory based manufacturing process centered on filament winding epoxy impregnated basalt fibers onto either: a) fully cured, or b) partially cured polyurethane liner. Fully curing the liner prior to filament winding forms a mechanical bond between the polyurethane and epoxy. Conversely, a semi-cured liner is capable of chemically bonding with the epoxy.

Preliminary experimental results from tubulars subjected to pure internal pressure indicate that a chemical interfacial bond delays the onset of burst failure in the pipe relative to a mechanical interfacial bond (13.23 MPa and 9.83 MPa, respectively). It is suspected that the polyurea compound, which is formed through the reaction between isocyanate in the polyurethane and amine in the epoxy curative agent, helps to distribute the stress in the composite structure after micro-matrix cracking occurs in epoxy matrix. Since there is no such interfacial compound formed in mechanically bonded specimens to help evenly distribute the stress, fiber fracture occurs at a lower pressure.

An unlined composite pipe was also tested, and found to undergo leakage failure at 7.27 MPa. Leakage failure is dominated by matrix degradation, however, the fibers in the composite structure still maintain signifcant load carrying capability. Therefore, a pipe commissioning process that loads a lined FRP pipe to the corresponding internal pressure associated with matrix degradation may provide the necessary micro-matrix cracks required for adequate venting of trapped interfacial volatiles.

c. Polyurethane-Epoxy Interface Adhesion: An Experimental Investigation

From chapter 3, evidence was provided that interfacial bond type (mechanical vs. chemical) may have an impact on the structural strength of the developed lined composite piping system. However, during manufacturing of the small-scale pipe specimens it was observed (in contrast to fully cured liners) that the semi-cured liners used to form a chemical bond were prone to ripping and consequently had to be handled delicately. Therefore, in order to optimize the pipe manufacturing process, an experimental fracture approach based blister testing was adopted in order to elucidate the influence of bond type on interfacial strength.

The results of this investigation illustrated that the mechanically bonded PU-epoxy specimens had an average fracture toughness of approximately 1173.5 J/m^2. Conversely, it was observed that the chemically bonded specimens did not exhibit any interfacial fracture, instead the polyurethane overlayer underwent extensive permanent deformation as it formed a large balloon-like blister; tests were terminated to prevent the blister from rupturing. Based on these results, it is evident that a chemically bonded interface is far superior to its mechanically bonded counterpart, and as such, chemical bonding should be the preferred interfacial joining method during pipe fabrication.

d. Polyurethane-Epoxy Interface Adhesion: A Finite Element Analysis

Future finite element analysis of the developed pipe may require modeling of a mechanically bonded PU-epoxy interface. To accomplish this goal, a numerical model was developed to simulate the start of debonding based upon experimentally deter-

mined fracture results of mechanically bonded blister samples. This analysis implemented a cohesive zone model, which requires two parameters, namely the cohesive separation energy and maximum cohesive tensile strength, to accurately model crack initiation of an interface. The cohesive separation energy is also termed the work of fracture and was experimentally determined to be G_{cn}=1173.5 J/m^2 in Chapter 4. Through numerical trials, it was determined that a maximum cohesive strength of 14.25 MPa was adequate to model the interface to best fit experimental data.It is anticipated that these values can be incorporated into future finite element investigations that require modeling of such an interface subjected to mode I loading conditions.

6.1 Recommendations for Future Work

Future analysis should include:

1. Further testing to explore the failure envelope of the lined composite pipe. The failure envelope of the lined composite pipe can be established by performing a series of tests with various loading ratios and determining the failure pressures. Furthermore, it is necessary to complete more pipe tests to further elucidate the influence of bond type on pipe strength.

2. Quantifying the uniformity of micro-matrix cracks introduced during the pipe commissioning process. The use of traditional measuring instruments such as extensometers and strain gauges cannot provide such information; however, full-field digital image correlation (DIC) may provide such a solution [1]. In DIC, speckles are applied to the surface of the composite pipe. Then using an industrial CCD camera, digital pictures of the unique pattern are captured before and during loading. Using these images, a robust analysis program computes

the surface strain maps. By correlating the strain mappings to specific loading conditions, the extent of matrix damage can potentially be evaluated.

3. Analysis of pipe integrity after long-term exposure to hydrocarbons. Thus far the pipes have been tested in their virgin state, however, to obtain a realistic measure of lifespan and performance, future experimental testing should be performed after exposing the specimens to hydrocarbons. This can be accomplished by soaking specimens in an aggressive medium for prolonged periods, followed by both fatigue and monotonic loading senarios.

4. Further verification of the cohesive zone parameters. This can be accomplished by experimentally testing a blister specimen with a different PU overlayer thickness, and determining the corresponding critical pressure for crack initiation and maximum blister height at debonding. If the above determined CZM parameters are accurate, then they should be capable of accurately modelling the new blister geometry. In addition, a parametric study also analyze the error attributed to uncertainty in the modulus of elasticity and Poisson's ratio on the numerical results.

5. Improving the ease of manufacturing chemically bonded pipe specimens. There are several possible options available, the first option involves altering the chemical formulation of the polyurethane such that there is an excess of isocyanate in the mixture. This allows one to fully cure the specimen, however the additional isocyanate would remain functional and therefore available to react with the epoxy resin. A second option involves using a coupling agent which would allow one to chemically bond a fully cured liner to the epoxy resin through a surface primer. Lastly, to improve the stiffness of the polyurethane while it is in a partially cured state one could add filler, which could potentially serve to increase abrasion resistence.

6. Investigating industrial implementation of the pipe design. The specimens fabricated in this investigation were based upon small scale laboratory procedures; however, as mentioned previously typical slurry transport pipes are usually within the 61 to 91 centimeter (24 to 36 inch) range. To accommodate such large diameters, it would be necessary to alter the manufacturing process. It is anticipated that a continuous extrusion process would be implemented to form the internal polyurethane liner. The semi cured liner would be extruded on to a collapsible mandrel. This mandrel-liner system would then be wound upon with epoxy impregnated fibers. Following winding, rapid curing of the epoxy resign would occur, after which the mandrel would collapse upon itself and automatically return to the beginning of the production line. Such filament winding systems with collapsible mandrels are currently used in industry today. Thus, by incorporating a continuous extrusion process into an innovative and mobile filament winding setup as suggested in [2], it may be possible to form indefinite pipeline lengths on-site, thus reducing the number of joints (relative to traditional steel pipelines), and limitations posed by transportation size restrictions. Future work should investigate the manufacturing and economic feasibility of such an implementation.

Bibliography

[1] Juss, K., P. Mertiny, Koltarski, J., "Detection of matrix cracking and leakage in FRPC tubes through digital image analysis," The 6th Canadian-International Composites Conference (CANCOM), 2007.

[2] Goldsworthy, W.B., Hardesty, E.E., "Method and apparatus for producing filament reinforced tubular products on a continuous basis," US Patent 3,579,402, 1971.

Chapter 7

Appendix: Sample ANSYS APDL Code

```
/TITLE,BLISTER TEST ANALYSIS
/PREP7
!---------elements
ET,1,PLANE182                    !*2D 4-NODE STRUCTURAL SOLID ELEMENT
KEYOPT,1,3,1                     !*AXISYMMETRIC

ET,2,PLANE182                    !*2D 4-NODE STRUCTURAL SOLID ELEMENT
KEYOPT,2,3,1                     !*AXISYMMETRIC

ET,3,TARGE169                    !*2D TARGET ELEMENT

ET,4,CONTA171                    !*2D CONTACT ELEMENT
KEYOPT,4,12,5                    !*ALWAYS BONDED CONTACT

!---------materials
EMAT1=21.5e6                     !*EMAT1=Young's Modulus of Material 1(Pa)
vMAT1= 0.44                      !*vMAT1=Poisson's Ratio of Material 1

MP,EX,1,EMAT1
MP,PRXY,1,vMAT1

EMAT2=2.9e9                      !*EMAT2=Young's Modulus of Material 2 (Pa)
vMAT2=0.42                       !*vMAT2=Poisson's Ratio of Material 2

MP,EX,2,EMAT2
MP,PRXY,2,vMAT2
!---------cmz
SMAX=14.25E6
Gcn=1173.5
DampingFactor=0.00028571

TB,CZM,3,1,1,CBDE
TBDATA,1,SMAX,Gcn,,,DampingFactor,

!---------geometery
t1=0.002                         !*t1=thickness of Material 1    (m)
t2=0.005                         !*t2=thickness of Material 2    (m)
len=.01508                       !*len=length of specimen        (m)
a=0.0075                         !*a=initial crack length        (m)
RECTNG,0,len,0,t1                !*DEFINE AREAS
RECTNG,a,len,0,-t2

LDIV,1,(a/len),,2,0
LDIV,3,(1-a/len),,2,0
L,8,10

A,4,10,9,1
A,10,3,2,9
ADELE,1,,,0

LSEL,S,LINE,,3,9,2               !*DEFINE LINE DIVISION
```

```
LESIZE,ALL,,,50

LSEL,S,LINE,,1,,
LSEL,A,LINE,,10,,
LESIZE,ALL,,,45

LSEL,S,LINE,,6,8,2
LESIZE,ALL,,,6

LSEL,S,LINE,,2,4,2
LSEL,A,LINE,,11
LESIZE,ALL,,,12

ALLSEL,ALL

!---------meshing
TYPE,2                          !*MESH AREA 2 (substrate)
MAT,2
LOCAL,11,0,0,0,0
ESYS,11
MSHAPE,0
MSHKEY,2
AMESH,2
CSYS,0

TYPE,1                          !*MESH AREA 3 (blister area)
MAT,1
ESYS,11
MSHAPE,0
MSHKEY,2
AMESH,3
CSYS,0

TYPE,1                          !*MESH AREA 4 (film)
MAT,1
ESYS,11
MSHAPE,0
MSHKEY,2
AMESH,4
CSYS,0

NSEL,S,LOC,X,a,len              !*TARGET ELEMENTS
TYPE,3
MAT,3
ESEL,S,TYPE,,2
NSLE,S
NSEL,R,LOC,Y
ESURF

TYPE,4                          !*CONTACT ELEMENTS
ESEL,S,TYPE,,1
```

```
NSLE,S
NSEL,R,LOC,Y
NSEL,R,LOC,X,a,len
ESURF

FINISH

/SOLU                          !*ENTER SOLUTION PROCESSOR
ANTYPE,STATIC                  !*SPECIFY ANALYSIS TO BE STATIC
NLGEOM,ON                      !*TURN NONLINEAR GEOMETRY EFFECTS ON
OUTRES,ALL,ALL                 !*WRITE ALL SOLUTION ITEMS FOR EVERY
                               !*SUBSTEP
ALLSEL,ALL

!*apply boundary conditions
NSEL,S,LOC,Y,-t2
D,ALL,ALL,0                    !*CONSTRAIN ALL D.O.F AT SELECTED NODES
ALLSEL, ALL                    !*SELECT EVERYTHING

!---------initial
Pcritical=844825.6             !*CRITICAL PRESSURE
Max_Initial_Pres=845825.6
LSEL,S,LINE,,1
NSLL,S,1
SF,ALL,PRES,Max_Initial_Pres
ALLSEL,ALL                     !*SELECT EVERYTHING
NLGEOM,ON                      !*TURN ON NON-LINEAR EFFECTS
SOLCONTROL,ON

NROPT,FULL                     !*FULL NEWTON-RAPHSON METHOD
AUTOTS,ON                      !*USE AUTOMATIC TIME STEPPING
NSUBST,50,50,50
TIME,1                         !*FIRST TIME STEP
SOLVE                          !*SOLVE LOAD STEP

!---------pcritical
Pressure_Inc=10000             !*CALCULATE PRESSURE INCREMENT
flag=1
i=2
/GOPR
*DOWHILE,flag                        !*DOWHILE flag>0
  load_step=i-1                      !*CALCULATE PREVIOUS LOAD STEP
  PARSAV,ALL
  ANTYPE,STATIC,REST,%load_step%     !*START AT END OF PREV. LOAD STEP

  PARRES,NEW
  current_pres=(Max_Initial_Pres+(i-1)*Pressure_Inc)
  *IF,current_pres,GT,(1.20*Pcritical),THEN
    flag=0
    *CYCLE
  *ENDIF
```

```
LSEL,S,LINE,,1
NSLL,S,1
SF,ALL,PRES,current_pres
ALLSEL,ALL                          !*SELECT EVERYTHING
NLGEOM,ON
SOLCONTROL,ON

NROPT,FULL
AUTOTS,ON

NSUBST,10,10,10
TIME,%i%

SOLVE

/POST1                              !*ENTER POSTPROCESSOR
ALLSEL,ALL                          !*SELECT ALL
ESEL,S,TYPE,,4                      !*SELECT CONTACT ELEMENTS ONLY
ETABLE,CON_STAT,CONT,STAT           !*ETABLE WITH CONT. ELEM. STATUS
*GET,num_of_elems,ELEM,0,COUNT      !*GET SIZE OF THE CURR. SELECTION
*GET,min_elem_num,ELEM,0,NUM,MIN
FINISH

/SOLU                               !*ENTER SOLUTION PROCESSOR
*DO,ii,1,num_of_elems,1
  hezzy=(ii+min_elem_num-1)
  *GET,cstat,ELEM,%hezzy%,ETAB,CON_STAT
  *IF,cstat,EQ,1.5,THEN
    flag=0                          !*DEBONDING: GET OUT OF LOOP
    ekill,%hezzy%
    FEM_Pcritical=current_pres      !*FEM PRESSURE AT INITIATION
  *ENDIF
 *ENDDO
 *IF,FLAG,EQ,1,THEN
  i=i+1
 *ENDIF
*ENDDO
```